Cell Reports

Article

Preproteins couple the intrinsic dynamics of SecA to its ATPase cycle to translocate via a catch and release mechanism

Graphical abstract

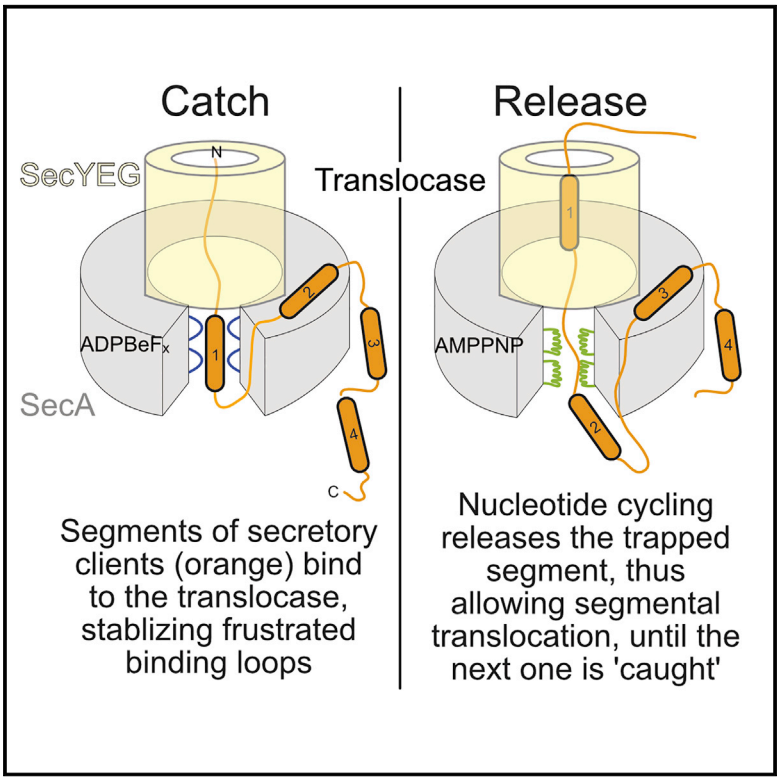

Highlights

- Preproteins couple the dynamics of the SecA ATPase motor to its preprotein clamp
- Preprotein binding causes increased motor dynamics leading to ADP release
- Nucleotide states subtly alter the intrinsic dynamics of Sec translocase
- Clients are translocated via a nucleotide-dependent "catch and release" mechanism

Authors

Srinath Krishnamurthy, Marios-Frantzeskos Sardis, Nikolaos Eleftheriadis, ..., Ana-Nicoleta Bondar, Spyridoula Karamanou, Anastassios Economou

Correspondence

tassos.economou@kuleuven.be

In brief

Combining biophysical and biochemical tools, Krishnamurthy et al. show how preproteins activate the intrinsically dynamic membrane-associated Sec translocase. Preprotein signal peptides close the clamp and mature domains increase motor dynamics. Nucleotides drive the translocase between conformational states that catch and release preproteins through frustrated prongs and lead to their translocation.

Krishnamurthy et al., 2022, Cell Reports *38*, 110346
February 8, 2022
https://doi.org/10.1016/j.celrep.2022.110346

CellPress

Cell Reports

CellPress
OPEN ACCESS

Article

Preproteins couple the intrinsic dynamics of SecA to its ATPase cycle to translocate via a catch and release mechanism

Srinath Krishnamurthy,[1] Marios-Frantzeskos Sardis,[1] Nikolaos Eleftheriadis,[1] Katerina E. Chatzi,[1] Jochem H. Smit,[1] Konstantina Karathanou,[2] Giorgos Gouridis,[1,3,4] Athina G. Portaliou,[1] Ana-Nicoleta Bondar,[2,5,6] Spyridoula Karamanou,[1] and Anastassios Economou[1,7,*]

[1]KU Leuven, University of Leuven, Rega Institute, Department of Microbiology and Immunology, 3000 Leuven, Belgium
[2]Freie Universität Berlin, Department of Physics, Theoretical Molecular Biophysics Group, Arnimallee 14, 14195 Berlin, Germany
[3]Molecular Microscopy Research Group, Zernike Institute for Advanced Materials, University of Groningen, Nijenborgh 4, 9747 AG Groningen, the Netherlands
[4]Structural Biology Division, Institute of Molecular Biology and Biotechnology (IMBB-FORTH), Nikolaou Plastira 100, Heraklion, Crete, Greece
[5]University of Bucharest, Faculty of Physics, Atomiștilor 405, 077125 Măgurele, Romania
[6]Forschungszentrum Jülich, Institute of Computational Biomedicine, IAS-5/INM-9, Wilhelm-Johnen Straße, 5428 Jülich, Germany
[7]Lead contact
*Correspondence: tassos.economou@kuleuven.be
https://doi.org/10.1016/j.celrep.2022.110346

SUMMARY

Protein machines undergo conformational motions to interact with and manipulate polymeric substrates. The Sec translocase promiscuously recognizes, becomes activated, and secretes >500 non-folded preprotein clients across bacterial cytoplasmic membranes. Here, we reveal that the intrinsic dynamics of the translocase ATPase, SecA, and of preproteins combine to achieve translocation. SecA possesses an intrinsically dynamic preprotein clamp attached to an equally dynamic ATPase motor. Alternating motor conformations are finely controlled by the γ-phosphate of ATP, while ADP causes motor stalling, independently of clamp motions. Functional preproteins physically bridge these independent dynamics. Their signal peptides promote clamp closing; their mature domain overcomes the rate-limiting ADP release. While repeated ATP cycles shift the motor between unique states, multiple conformationally frustrated prongs in the clamp repeatedly "catch and release" trapped preprotein segments until translocation completion. This universal mechanism allows any preprotein to promiscuously recognize the translocase, usurp its intrinsic dynamics, and become secreted.

INTRODUCTION

Protein machines modify, reshape, disaggregate, and transport nucleic acids and polypeptides (Avellaneda et al., 2017; Flechsig and Mikhailov, 2019; Kurakin, 2006) by converting between auto-inhibited and active states commonly relying on intrinsic structural dynamics (Nussinov et al., 2018). A fascinating paradigm is the bacterial Sec translocase that secretes preprotein clients across the inner membrane. Its SecA ATPase subunit, a four domain Superfamily 2 helicase (Figure S1A), binds non-folded clients, nucleotides, lipids, chaperones, and the SecYEG channel (De Geyter et al., 2020; Rapoport et al., 2017; Tsirigotaki et al., 2017a). A multi-tiered intrinsic dynamics nexus of sub-reactions activates the translocase (Corey et al., 2019; Gouridis et al., 2013; Krishnamurthy et al., 2021; Sardis and Economou, 2010), requiring minor energetic input from ligands. While partners and nucleotides prime the dynamics landscape of the translocase, ~500 loosely conserved clients activate it at the expense of energy via a universal mechanism (Tsirigotaki et al., 2017a).

Protein intrinsic dynamics and disorder are multi-leveled (Henzler-Wildman et al., 2007; Yang et al., 2014) and essential for a protein assembly and interactions (Dunker et al., 2002; Fuxreiter et al., 2014): motions between subunits (quaternary), within a chain (global), of a domain (rigid body), and of segments (local). It is unclear how intrinsic dynamics couple allostery to protein function (Loutchko and Flechsig, 2020; Zhang et al., 2019), even less so in multi-liganded/partner enzymes that operate hierarchically, like the Sec translocase.

Cytoplasmic SecA is dimeric, ADP-bound and quiescent, and chaperones clients (Sianidis et al., 2001). Its helicase motor (comprising nucleotide binding domains [NBDs] 1/2) is fused to an ATPase-suppressing C-domain and a preprotein binding domain (PBD; rooted via a stem in NBD1; Figure S1A). The PBD intrinsically rotates from a distal "wide-open" position toward NBD2 ("closed") (Ernst et al., 2018; Krishnamurthy et al., 2021; Sardis and Economou, 2010; Vandenberk et al., 2019) to clamp mature domains (Bauer and Rapoport, 2009). SecYEG binding (Figure 1AII, "primed") enhances local dynamics in

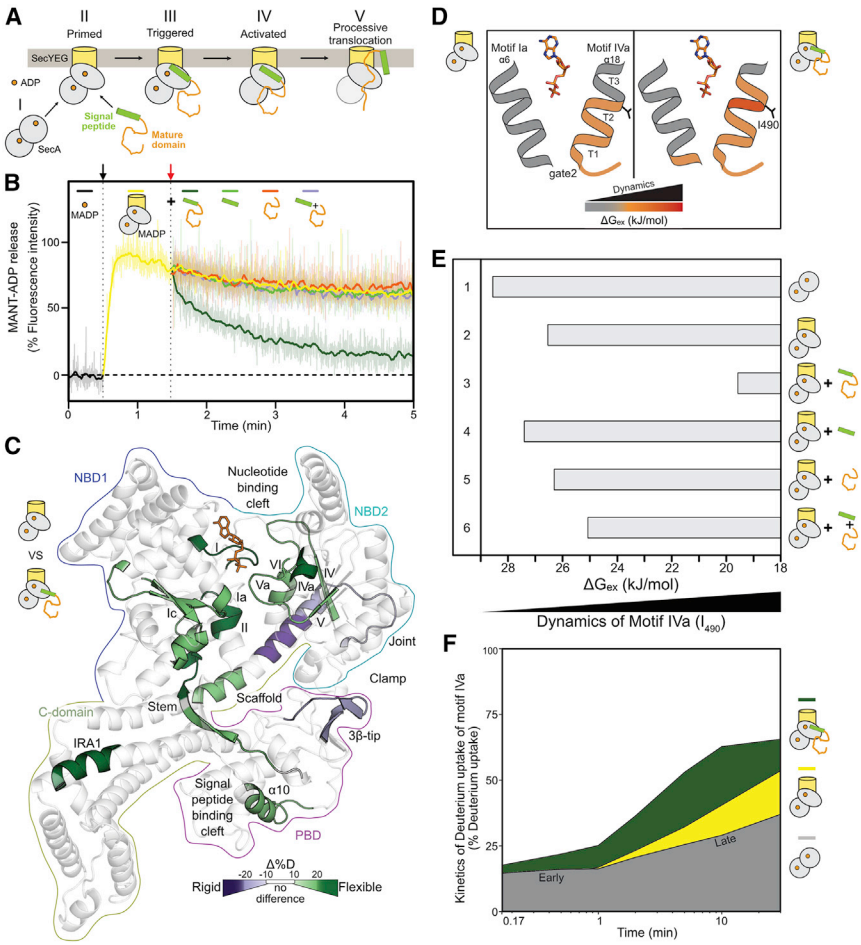

Figure 1. Preproteins induce ADP release by enhancing motor dynamics

(A) Cytoplasmic ADP-bound, quiescent $SecA_2$ (I) binds asymmetrically to SecYEG through the active protomer (II, gray oval). The preprotein is targeted to the translocase through bivalent signal peptide or mature domain binding. Signal peptide binding alone "triggers" (III), yet only preprotein binding activates (IV), the translocase for ATP hydrolysis cycles that result in processive translocation (V).

(B) ADP release assay. The fluorescence intensity of MANT-ADP increases upon binding to the translocase (black arrow). Reactions were chased (red arrow) with the indicated ligands (see STAR Methods). The drop in fluorescence intensity corresponds to the MANT-ADP release from SecA. Transparent lines: raw fluorescence traces (n = 3–4). solid lines: smoothened data (LOWESS). Preprotein: $proPhoA_{1\text{-}122}$, mature domain: $PhoA_{23\text{-}122}$.

(C) Effect of $proPhoA_{1\text{-}122}$ binding on the local dynamics (HDX-MS) of SecYEG:$SecA_2$:ADP. D uptake differences between SecYEG:$SecA_2$:ADP (top pictogram: "reference") and SecYEG:$SecA_2$:ADP:preprotein (bottom pictogram: "test") shown. Purple: decreased; green: increased dynamics; no difference: transparent gray. ADP: orange sticks. Domains are contoured.

(D) ΔGex values representing protein dynamics were calculated by PyHDX from HDX-MS data (Smit et al., 2021a) and mapped onto a cartoon of the closed-gate2 state with its two helices comprising helicase motifs Ia (α6) and IVa (α18; three turns). Dynamics of SecYEG:$SecA_2$:ADP in preprotein free (left) and bound (right) state are shown. I_{490} (between turns two and three) reports on motif IVa dynamics. ADP: orange sticks. See also Figure S1D.

(E) ΔGex values (from D) for I_{490} (motif IVa) determined under the indicated conditions. Decreased ΔGex values: increased dynamics.

(F) D uptake kinetic plots of peptide aa488-501 (motif IVa), shown as a percentage of its full deuteration control (Table S1), for $SecA_2$:ADP (gray), SecYEG:$SecA_2$:ADP (yellow), and SecYEG:$SecA_2$:ADP:preprotein (green). Labeling timepoints (0.17, 0.5, 1, 2, 5, 10, and 30 m) and SD values (<2%) not shown. n = 3.

SecA's motor, scaffold, and stem (Figure S1A) (Krishnamurthy et al., 2021). Asymmetric $SecA_2$ binding to the channel increases clamp dynamics and interconversion between open and closed states in the channel-bound protomer ("active"). The *primed* translocase has 10-fold higher affinity for clients (Gouridis et al., 2009, 2013; Hartl et al., 1990) but low ATP turnover (Fak et al., 2004; Keramisanou et al., 2006; Krishnamurthy et al., 2021; Sianidis et al., 2001). It becomes fully activated only after clients bind to SecA on sites distinct for signal peptides (in PBD bulb) and mature domains (on and around PBD stem; Figure S1B) (Chatzi et al., 2017; Gelis et al., 2007; Sardis et al., 2017). Signal peptides promote a low activation energy conformation (Figure 1AIII; "triggered"), *activating* the ATPase (Figure 1AIV) for *processive* translocation (Figure 1AV).

We previously developed a multi-pronged approach to study the intrinsic dynamics of SecA and how these underlie conversion from a quiescent to a primed state (Karathanou and Bondar, 2019; Krishnamurthy et al., 2021; Vandenberk et al., 2019). We probed *global* dynamics or H-bond networks with atomistic molecular dynamics (MD) simulations and graph analysis, PBD clamp motions by single-molecule Förster resonance energy transfer (smFRET) and *local* dynamics by hydrogen deuterium exchange mass spectrometry (HDX-MS). These tools are used here under translocation conditions, identical to those used for biochemical dissection, without detergents that monomerize and alter SecA dynamics (Ahdash et al., 2019; Or et al., 2002).

We reveal that preproteins achieve translocation by temporarily bridging the otherwise uncoupled intrinsic dynamics of the SecA motor and clamp. Binding on the primed translocase (Figure S1B) (Sardis et al., 2017), signal peptides promote clamp closing and mature domains drive enhanced dynamics that facilitate ADP release. Fresh ATP binding and hydrolysis, sensed through the γ-phosphate, promote distinct motor states and affect four frustrated prongs that line the clamp and undergo transient binding and release cycles on multiple islands on the client. Clients couple clamp motions to distinct nucleotide-regulated motor states. Upon completion of translocation, a

client-less translocase can no longer release ADP and becomes quiescent.

RESULTS

Preprotein-stimulated ADP release from the helicase motor

To stimulate ATP turnover at the translocase clients destabilize the SecA:ADP state. We tested this by monitoring the binding and release of MANT-ADP from SecYEG:$SecA_2$ upon preprotein addition (Figure 1B). The fluorescence intensity of MANT-ADP increases upon binding to SecA (37°C; Figure 1B; black arrow) (Galletto et al., 2005; Karamanou et al., 2005; Krishnamurthy et al., 2021), and it remains high (Figure 1B, yellow line), indicating tight ADP binding. Preprotein addition (proPhoA$_{1\text{-}122}$; Chatzi et al., 2017) (Figure 1B, orange arrow) causes a drop in fluorescence intensity (green line), indicative of MANT-ADP release. Release is not observed in soluble $SecA_2$ (37°C; Figure S1CI) nor at 10°C with channel-bound $SecA_2$ (II). ATP excess on channel-bound $SecA_2$ is as efficient in MANT-ADP release as proPhoA$_{1\text{-}122}$ (2 mM; 37°C; III), while signal peptide (Figure 1B, green) or mature domain (orange) alone, or combined *in trans* (purple), at concentrations several fold over their K_d, are not. Since only physiological conditions induce ADP release, this reaction is *on pathway*.

Preprotein-enhanced motor dynamics underlie ADP release

To study if preprotein-stimulated ADP release correlates with changes in the local dynamics of SecYEG:$SecA_2$:ADP, we used HDX-MS and derived Gibbs free energy of exchange per residue (ΔG_{ex}), which maps flexible or rigid regions (Figure S1D) (Krishnamurthy et al., 2021; Smit et al., 2021a).

To quantify the effect of preprotein binding on translocase dynamics, we compared the deuterium (D) uptake of SecYEG:$SecA_2$:ADP with (Figure S1D, right) or without (left; reference) preprotein and derived a ΔD uptake map. Preprotein binding enhanced dynamics of the motor (at helicase motifs [roman numerals] and parallel β-sheets; Figure 1C; green hues; Figure S1E), the mature domain (IRA1, stem) and signal peptide (PBD$_{\alpha 10}$; Figures S1A and S1D) binding sites (Keramisanou et al., 2006). In parallel, it decreased dynamics in the joint/scaffold start and the 3β-tip$_{PBD}$ (purple hues). The effects in the motor occuring far from preprotein binding sites (Figure S1B) are likely allosteric. As preprotein did not significantly alter soluble $SecA_2$ dynamics (Table S1), these effects must be *on pathway*.

Motor motifs I, II, and Va directly bind ATP phosphates (Papanikolau et al., 2007) (Figure S1E, left), while motifs IV and V are important parallel β-strands of NBD2. Motifs Ia and IVa form the lateral gate2, which occupies closed or open states affecting NBD1 and 2 association (Figure S1E, right) and regulate access to the nucleotide cleft (see below) and ATP hydrolysis (Figure S1E, left) (Karamanou et al., 2007). Increased dynamics at these motifs indicates weakened nucleotide contacts in the motor (Figure 1B).

In conclusion, preprotein binding alters motor dynamics at internal and peripheral gate2 helicase motifs (Figures 1D–1F), drives ADP release (Figure 1B), and restarts the ATPase cycle.

Motif IVa of gate2 senses ligands via its intrinsic dynamics

Motif IVa$_{gate2}$ is intriguing. It has elevated basal dynamics, is sensitive to multiple interactants (Krishnamurthy et al., 2021), and is located between the ADP-binding motif Va and motifs IV and Vb on NBD2 β-strands (Figure S1E). It comprises a flexible linker followed by a three-turn helix with a constantly dynamic first half (Figure 1D, left, orange; Figure S1D, left) and a conditionally dynamic second half (turns two–three). Preprotein binding increased dynamics specifically of I_{490} (Figures 1D and S1D, right), yielding a quantitative assay. Channel binding marginally affects dynamics of $SecA_2$:ADP (Figure 1E, compare lane 2 to 1). Preprotein binding to SecYEG:$SecA_2$:ADP significantly further enhances dynamics (lane 3), while signal peptides (lane 4) or mature domains (lane 5) added alone, or together (lane 6), cause minor effects.

Motif IVa shows biphasic D uptake kinetics that suggest modulation of its energy landscape in two differentially flexible conformational steps (Figure 1F, gray), due to varying D uptake kinetics in different regions of the analyzed peptide or combined H bonding and solvent accessibility effects. Channel binding increased selectively the second-phase dynamics (yellow). Preprotein added on top increased both phases (green), suggesting a major loosening of motif IVa's conformational landscape. Neither step alone is sufficient; together they complete activation of the translocase, and preprotein could not be replaced either by signal peptide (Figure S1FI) nor by mature domain (II) added alone or together *in trans* (III).

Therefore, motif IVa of gate2 senses clients via its intrinsic dynamics.

ADP-antagonized, signal peptide-regulated motif IVa dynamics

The contribution of each preprotein moiety to activating the translocase was probed next. proPhoA's signal peptide marginally affected the dynamics of SecYEG:$SecA_2$:ADP (Figures 1E and S1FI; Table S1). Presuming that bound ADP antagonized subtle dynamics effects, we tested signal peptide binding on SecYEG:$SecA_2$. This time we observed increased motif IVa localized dynamics: at turn two of motif IVa and the middle of the scaffold (Figure 2A). Time-dependent dynamics of motif IVa revealed that signal peptide binding increased the dynamics of the early but not the late phase (Figure 2B, compare line to shaded yellow), albeit less than did the preprotein (compare line to shaded green; Figure S2A). This was corroborated by I_{490} dynamics (Figure S2B).

The measurable but minor effect the signal peptide had on SecA's conformational landscape (compared to the preprotein effect), primarily at motif IVa$_{gate2}$ likely underlies triggering (Figure 1AIII).

Signal peptide-induced translocase triggering occurs via motif IVa dynamics

To understand how signal peptides control translocase dynamics via motif IVa, we used PrI (protein localization) mutants in SecA(PrlD) or SecY(PrlA). These gain-of-function mutants secrete clients devoid of signal peptides (Figure S2E) (Flower et al., 1994; Huie and Silhavy, 1995) by structurally mimicking

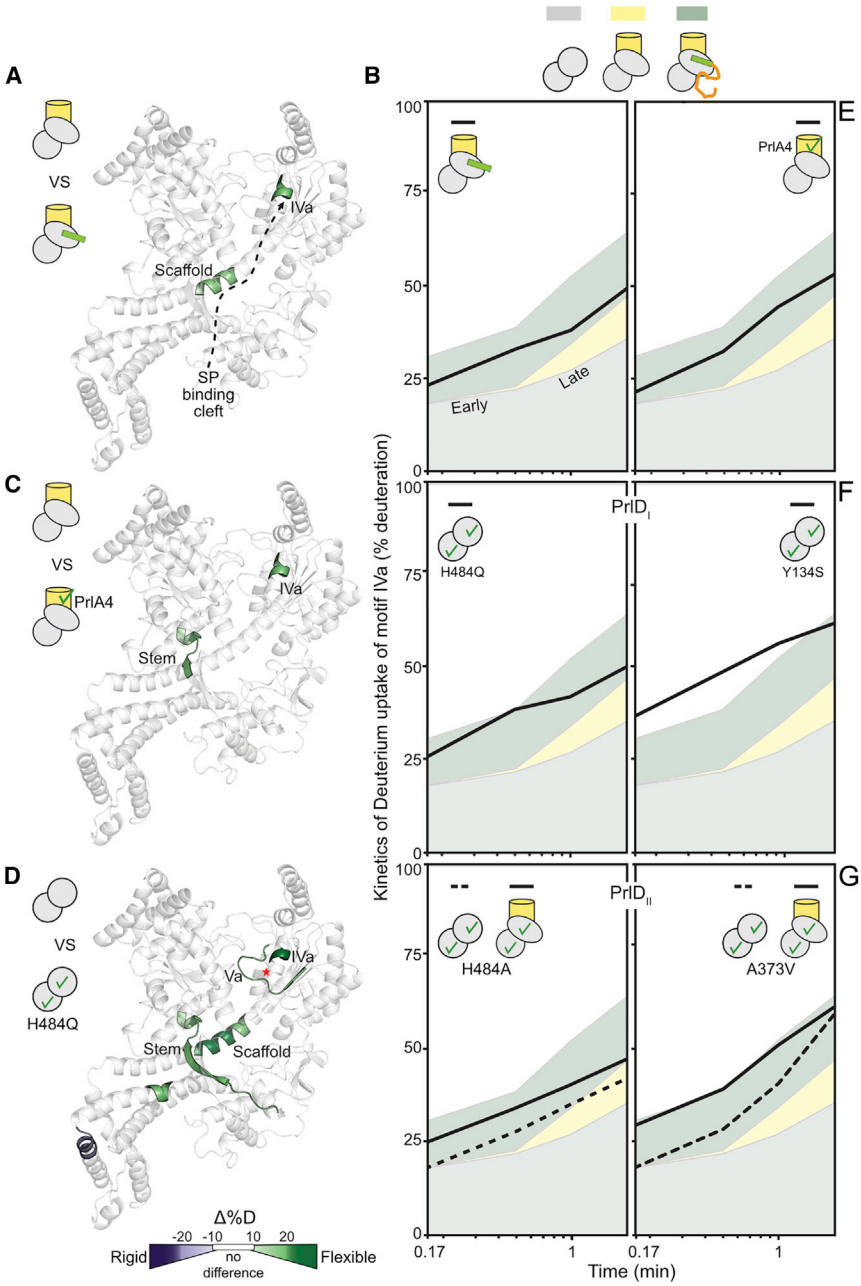

Figure 2. Signal peptides trigger the translocase by enhancing gate2 dynamics

(A) Long-range signal peptide effect (dashed arrow) on the local dynamics of channel-primed $SecA_2$. Regions showing differential D uptake in SecYEG:$SecA_2$:signal peptide compared to SecYEG:$SecA_2$ are mapped onto a single SecA protomer, as indicated. Only increased dynamics were observed (green).

(B) D uptake kinetic plots of a motif IVa peptide (aa488-501, as in Figure 1E but without ADP) in SecYEG:$SecA_2$:signal peptide were compared with the kinetics of the same peptide from $SecA_2$ (gray), SecYEG:$SecA_2$ (yellow), and SecYEG:$SecA_2$:preprotein (green). The ADP-bound (Figure 1E) and free (Figure S2A) states had minor differences. Selected kinetic regime focuses on timepoints (10 s, 30 s, 1 m, 2 m) that show the maximum differences; SD values (<2%) not shown. n = 3. See also Figure S2A.

(C and D) Local dynamics of $SecY_{PrlA4}EG$:$SecA_2$ (red asterisk; test) compared to those of SecYEG:$SecA_2$ (control) (C), of SecA $(H484Q)_2$ (test), and to those of $SecA_2$ (control) (D), shown as in (A).

(E–G) D uptake kinetics of motif IVa peptide, as in (B), in $SecY_{PrlA4}EG$:$SecA_2$ (E) or in $SecA_{PrlD}$ mutants (I, F; II, G) in solution.

the signal peptide-induced triggering (Figures 1AIII and S2D, lanes 3–5) (Gouridis et al., 2009). Some are triggered even without a channel (Figure S2D, lanes 4–5; hereafter $SecA_{PrlDI}$).

Three $SecA_{PrlD}$ hotspots line both walls of gate2: H484 and A488 in motif IVa, juxtapose Y134 of motif Ia (Figure S2C). Others lie in adjacent motifs, e.g., A507 (motif Va). Minor side chain changes in Y134 or H484 mimic the binary effect of channel plus signal peptide binding, in the absence of either. We screened mutant derivatives to dissect the two ligand effects on H484. Both *secA(H484Q)* and *secA(H484A)* display a Prl phenotype (Figure S2E, lanes 5–6). Yet, unlike SecA(H484Q) (Figure S2D, lane 5), triggering of SecA(H484A) requires channel binding (lanes 6–7; hereafter $SecA_{PrlDII}$).

Wild-type $SecA_2$ bound to SecYEG or $SecY_{PrlA4}EG$ exhibited similar dynamics. The latter displayed additionally elevated dynamics in motif IVa and the stem (Figure 2C). Similarly, compared to $SecA_2$, SecA$(H484Q)_2$ exhibited elevated motif IVa, stem and scaffold dynamics in the absence of channel or preprotein (Figure 2D).

$SecY_{PrlA4}EG$:$SecA_2$ (Figure 2E) and all $SecA_{PrlDI}$ mutants alone (Figure 2F) displayed elevated early phase dynamics of motif IVa, like those seen by signal peptide or preprotein in the wild type (Figure 2B). Motif IVa's dynamics in $SecA_{PrlDII}$ mutants (Figure 2G; dashed line) increased significantly upon channel binding (solid line), thus explaining their channel-dependence for triggering.

Fine modulation of gate2$_{\text{motif IVa}}$ dynamics is an essential aspect of signal peptide-mediated translocase triggering.

Signal peptides promote closing of the preprotein clamp

We hypothesized that signal peptides influence motif IVa dynamics and translocase triggering by controlling PBD rotation around its stem and tested this using smFRET (Krishnamurthy et al., 2021; Vandenberk et al., 2019). Fluorophores on PBD and NBD2 monitor these clamp-forming domains coming close

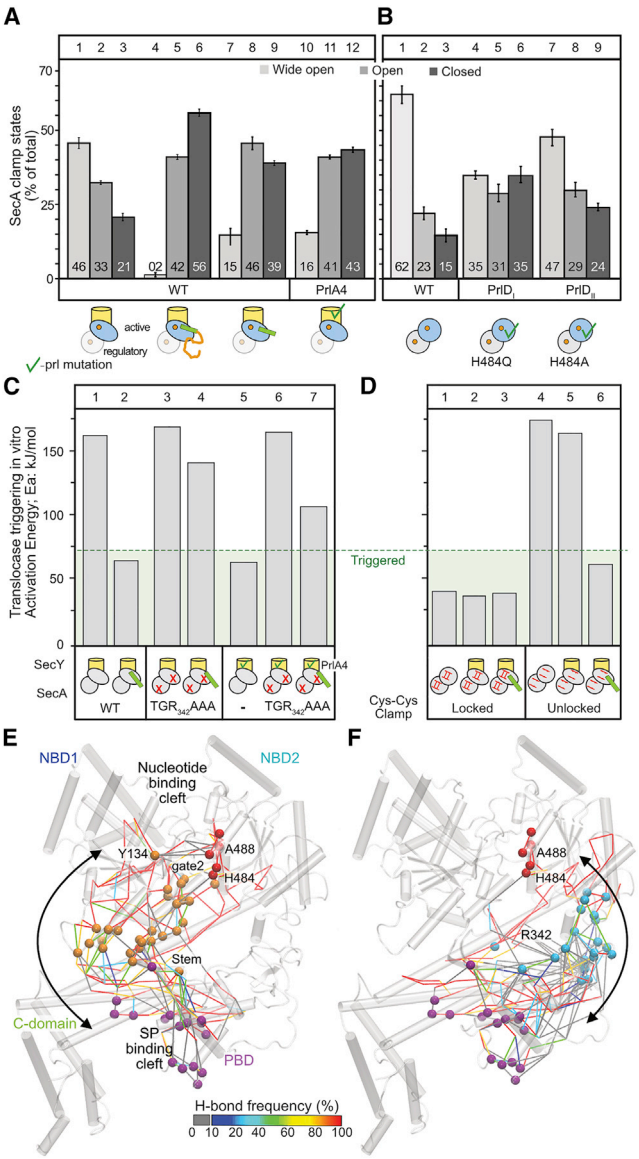

Figure 3. Clamp closing underlies translocase triggering

(A and B) The distribution of population percentages of the preprotein clamp in channel-bound (A) and free (B) $SecA_2$, determined by confocal smFRET (Krishnamurthy et al., 2021). In channel-bound conditions, only data for the active, channel-bound protomer (blue oval) are shown. n ≥ 3; mean (±SEM). Also see Figure S3.

(C and D) Activation energy (E_a) of wild-type SecA, SecA($TGR_{342}AAA$) (C) and a double cysteine SecA derivative (D) under the indicated conditions; oxidized = locked closed; reduced = unlocked open clamp.

(E and F) H bond pathways connecting motif IVa (red) to the signal peptide cleft (purple) through the stem (E; orange), or the PBD-NBD2 interface (F; cyan), derived from graph analysis of MD simulations of $ecSecA_{2VDA}$ with an open gate2. PDB:2VDA

or apart (high and low FRET, respectively; Figures S3A and S3B).

In SecYEG:$SecA_2$ the PBD of the active protomer samples all three states, with a preference for the wide open (Figure 3A, lanes 1–3; Figure S3BIIa). Preprotein binding closes the clamp (i.e., open plus closed states) in 98% of the active protomers (lanes 4–6), irrespective of ADP (Figure S3BIII). Signal peptides alone can replicate this in 85% of the active protomers (Figure 3A, lanes 7–9). The already triggered $SecY_{PrlA4}EG$:$SecA_2$ exhibits clamp closing in the absence of preprotein or signal peptide (lanes 10–12). Signal peptide-driven clamp closing (Figure 3A, lanes 7–9) is not accompanied by detectable secondary structure or flexibility changes inside the PBD or nucleotide cleft (Figure 2A). This rigid body motion is rather uncoupled from nucleotide turnovers in the helicase motor (see below). The freely diffusing wild-type $SecA_2$ maintains its clamp equilibrium at the wide-open state (Figure 3B, lanes 1–3) and signal peptides cannot close it (Figure S3BI). In contrast, in diffusing, spontaneously triggered $SecA_{PrlDI}$, clamp equilibria shift toward closed states in the absence of channel or signal peptides (Figure 3B, lanes 4–6) but less so in $SecA_{PrlDII}$ that require the channel for triggering (lanes 7–9; Figures S3BIVb and S3BIVc and S3C).

To test if NBD2-PBD interaction in the closed clamp is functionally important, we mutated the conserved 3β-tip_{PBD} that binds NBD2 (Figure S3A). The generated SecA($TGR_{342}AAA$) failed to become triggered by signal peptide (Figure 3C, lane 4), $SecY_{PrlA4}$ (lane 6), or their combination (lane 7). SecA($TGR_{342}AAA$) binds to channel/preproteins (Figure S4A) yet fails to stimulate its ATPase, secreted *in vitro* or *in vivo* (Figures S4B–S4D).

Furthermore, we locked the clamp in the closed state through engineered disulfides (Chatzi et al., 2017; Sardis et al., 2017) and tested functionality. The $SecA_{locked\ closed}$ was permanently triggered, independently of channel or preprotein (Figure 3D, lanes 1–3), akin to $SecA_{PrlDI}$ mutants (Figure S2C, lanes 4–5). Reduction of the disulfide reinstated a *channel plus preprotein* requirement for triggering (Figure 3D, lanes 4–6).

Signal peptide-driven clamp closing and increased motif IVa dynamics underlie translocase triggering.

The signal-peptide cleft crosstalks to motif IVa via two main H-bond pathways

To determine how clamp closing might allow the signal peptide binding cleft to crosstalk with motif IVa, we determined the H bond networks, including water-mediated bridging, between the two allosterically connected sites. In all simulations motif IVa (Figures 3E and 3F, red spheres) interconnected within a local H bond network extending to most SecA's residues (Krishnamurthy et al., 2021). Graph analysis determined the most frequently visited or shortest possible H bond pathways that could be potentially altered along the reaction coordinate of SecA. Through these the signal peptide cleft in PBD (purple spheres) could communicate with motif IVa. Two main routes were proposed. One, via the $NBD2_{Joint}$/PBD_{Bulb} interface of the closed clamp (Figure 3F, cyan spheres), was experimentally tested above. The other, via the PBD_{Stem}/a8 interface that binds mature domains and interconnects to the second half of gate2 (Y134; Figure 3E, orange spheres), was tested below.

The signal-peptide cleft crosstalks to motif IVa through the stem/α8 interface

During open-closed state transitions the stem/α8 interface, which binds mature domains (Chatzi et al., 2017), is

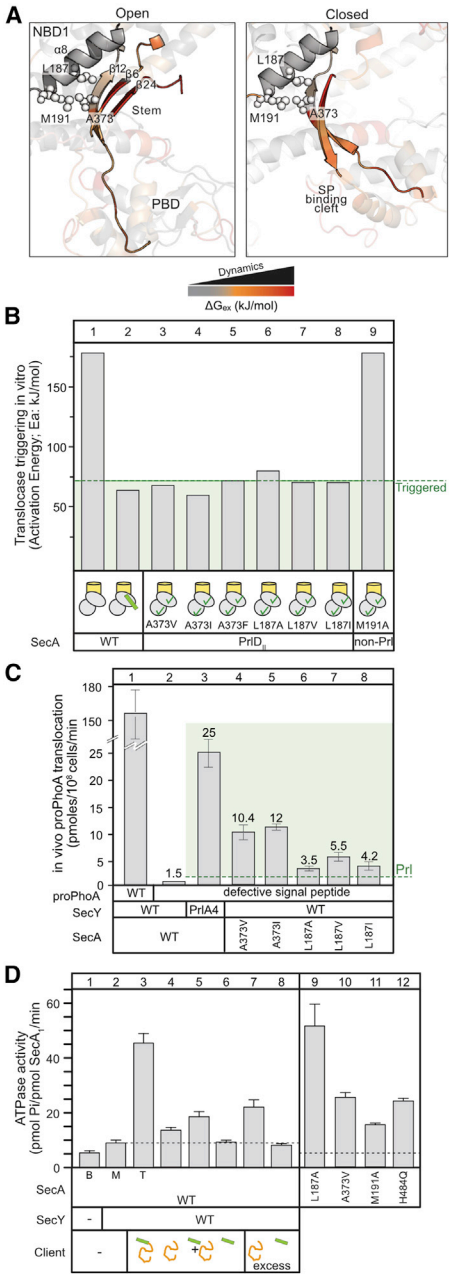

Figure 4. Mature domain-driven ADP release and ATP turnovers

(A) Structure (aligned on NBD1) and residues at the stem/α8 region including $\beta24_{C\text{-tail}}$. ΔG_{ex} values are shown for the SecYEG:$SecA_2$:preprotein state in the open (left; *ec*$SecA_{2VDA}$; PDB:2VDA) or closed (right; *ec*$SecA_{2VDA}$ MD model) clamp.

(B) Activation energy (E_a) of indicated stem $SecA_{PrlDII}$ mutants in channel-primed states, compared to wild-type translocase (as in Figure 3B).

(C) *In vivo* translocation of proPhoA or pro(L8Q)PhoA (defective signal peptide) by the indicated translocases. n = 6; mean values (±SEM).

(D) The ATPase activity of SecA in basal (B), membrane bound (M), and translocating conditions (T). Signal peptide (30 or 60 [excess] μM; mature domain (PhoAcys-; 20 or 40 [excess] μM). n = 3–6; mean values (±SEM).

conformationally altered (Figures 4A and S3A). As this interface is pried open, local hydrophobic stem β strands/α8 interactions likely change. The interface extends to a three strand β-sheet with the highly dynamic $\beta6_{Stem}$ and $\beta24_{C\text{-tail}}$ and involves $L187_{\alpha8}$ that packs against A373 of $\beta12_{Stem}$ (Figure 4A).

To alter hydrophobic packing at the stem/α8 interface, we substituted $A373_{Stem}$ with large hydrophobic residues (V, I, F) and $L187_{\alpha8}$ with V, I, A. All derivatives displayed PrI phenotypes *in vitro* ($SecA_{PrlDII}$; Figure 4B, lanes 3–8) or *in vivo* (Figure 4C, lanes 6–8), with L187A as the weakest one. A373V has been the only known PrI outside the nucleotide binding cleft (Flower et al., 1994; Huie and Silhavy, 1995). M191A (a control), located one turn after L187 at the end of α8 and of the stem/α8 interface (Figure 4A), was not a PrI (Figure 4B, lane 9). All derivatives were functional *in vivo* (Figure S4E).

Signal peptides may alter hydrophobic packing at the mature domain binding patch on the stem/α8 interface.

Binding of mature domains drives ADP release and ATP turnover

Mature domains bind to the stem/α8 interface (Chatzi et al., 2017) (Figure S1B, orange surface). Yet, only preproteins stimulate ADP release (Figure 1B) and ATP turnover on the translocase (Figure 4D, lane 3) (Karamanou et al., 2007). Alone (lane 4; in excess: lane 7) or with signal peptide added *in trans* (lane 5), mature domains can poorly stimulate the ATPase (1.5, 2, and 3-fold, respectively). In contrast, the signal peptide cannot (lane 6; in excess: lane 8). Mature domains alone marginally increase the local dynamics of the helicase motor in SecYEG:$SecA_2$:ADP (Figure S4F). Minor effects are also seen upon *trans* addition of mature domain plus signal peptide (Figure S4G), thus explaining their inability to fully stimulate the ATPase when the two preprotein moieties are unconnected.

We presumed that signal peptides might optimize the stem/α8 interface for mature domains to bind and stimulate ATP turnover. So, we screened for mutant derivatives at this interface with high basal ATPase activity, mimicking the mature domain-bound state. L187A and A373V ($SecA_{PrlDI}$; Figure 4B) displayed elevated ATPase compared to free $SecA_2$ (Figure 4D, lanes 9–10), while derivatives at the back of α8 were non-functional (Figures S4H–S4J).

The conformational effects on stem/α8 and the motor ATPase seem coupled. The mature domain binding site residue M191 (Figure 4A) disentangled them. Freely diffusing SecA(M191A) displayed elevated basal (Figure 4D, lane 11) and hyper-stimulated translocation (Figure S4K, lane 5) ATPase but was neither a PrI (Figure 4B, lane 9) nor had changed motif IVa dynamics (Table S1). Stem/α8 interfacial residues appear critical for mature domains to control ADP release from the motor.

The roles of signal peptides and mature domains in translocase activation are inter-connected but divergent and converge at stem/α8. This hub couples conformational cues from signal peptide-driven clamp closing to promote mature domain binding, ADP release, and motif IVa dynamics in the motor.

Nucleotides finely control the intrinsic dynamics of SecA

Co-ordinated signal peptide/mature domain docking releases ADP from SecA, allowing fresh ATP binding. Using analogs as

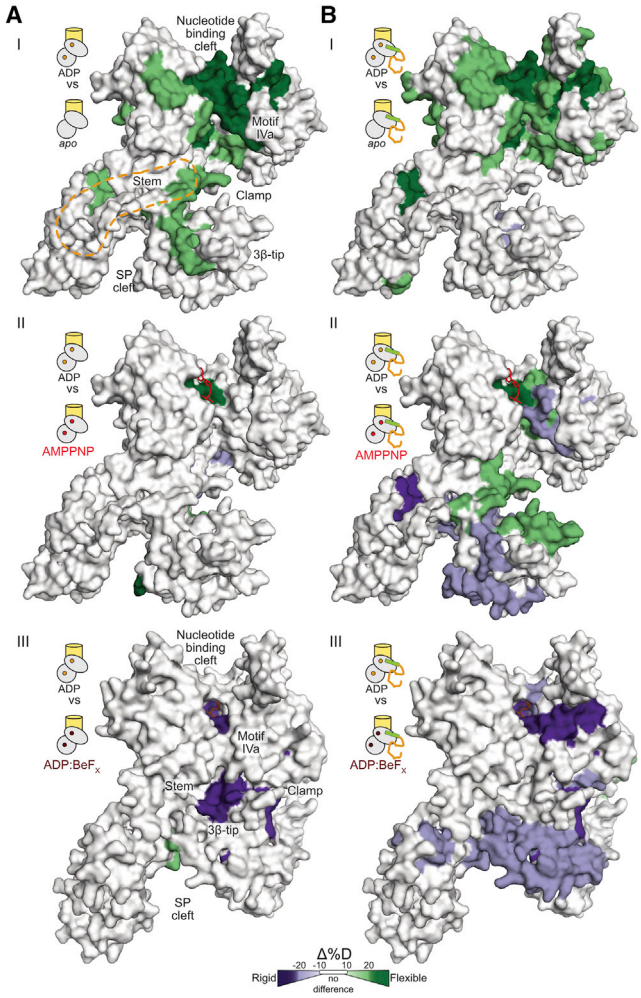

Figure 5. Nucleotide states and preproteins drive distinct translocase conformations

(A and B) The local dynamics (differential D uptake) of the SecYEG:SecA$_2$ at the indicated nucleotide state (I, II and III; "test") were compared to SecYEG:SecA$_2$:ADP ("reference"), in the absence (A) or presence (B) of preprotein. Orange dashed line in (A) I: PatchA. I and II mapped on surface representations of a protomer of *ec*SecA$_{2VDA}$ (open clamp; PDB:2VDA) and *ec*SecA$_{3DIN}$ (III; closed-flipped clamp; PDB:3DIN).

mimics of ATPase cycle stages we examined how they modulate SecYEG:SecA$_2$ dynamics using HDX-MS (Figure S5A). Nucleotides bind in a positively charged cleft using residues from both NBD1 and 2, mostly NBD1; β and γ-phosphates also contact NBD2 (Figure S5B) (Krishnamurthy et al., 2021; Papanikolau et al., 2007). We monitored the dynamics of the ADP (2 mM; 10^4-fold excess over K_d), apoprotein (i.e., empty cleft due to preprotein binding; Figure 1B), ATP (mimic: non-hydrolyzable AMPPNP), and ATP hydrolysis transition (mimic: ADP:BeF$_X$) (Zimmer et al., 2008) states. SecYEG:SecA$_2$:ADP dynamics were compared to all other states (Figures 5 and S5C; "reference," top versus bottom).

The suppressed SecA$_2$:ADP dynamics are somewhat relieved by channel priming (Krishnamurthy et al., 2021). Preprotein binding releases bound ADP (Figure 1B) and causes widespread elevated dynamics in the motor and localized ones in the stem, scaffold, IRA1, and PBD (Figure 5AI). The dynamics of SecYEG:SecA$_2$:AMPPNP and SecYEG:SecA$_2$:ADP differ marginally (Figures 5AII and S5CII). ADP:BeF$_X$ stabilizes additionally the motor (motifs I, IVa, V/Va) and the clamp (stem, α13, and the 3β-tip$_{PBD}$ that binds NBD2; Figure 5AIII). Motif Va harbors the R509 finger, crucial in γ-phosphate recognition and regulation of motor conformations (Keramisanou et al., 2006). Our results agree with the crystal structure of SecYEG:SecA:ADP:BeF$_x$ (Figure S6A) (Zimmer et al., 2008) where PBD$_{bulb}$ and NBD2 home into each other while PBD$_{3β\text{-}tip}$ flips toward NBD2$_{motifIVa}$, salt-bridging R342 to E487 (Figures S6B and S6C; Video S1). Conversion to the ADP state reverses rigidification through minor local changes (Figure S6DVIII). Some of these intra-protomeric changes enhance dynamics of the dimerization interface (Figure S5CI), suggesting preparation for dissociation (Gouridis et al., 2013). These effects are specific to channel-bound SecA$_2$. ADP:BeF$_X$ contacts in the soluble SecA$_2$ motor are weak (Table S1) with higher dynamics than ADP (Figure S6DIV).

The Q motif, that tightly binds the immutable adenine ring (Figure S1E), showed negligible dynamics in the presence of nucleotide consistent with similar motor affinities for ATP analogs. It is the mutable γ-phosphate in AMPPNP and ADP:BeF$_X$ that bind to NBD2 and stabilize different motor conformations, while ADP does not (Figures S1E and S5A). Missing γ-phosphate contacts weaken NBD2-ADP association, allow higher nucleotide mobility inside the pocket, and increase motif I dynamics (Figure S6DVIII).

Despite only minor chemical differences, nucleotides stabilize unique conformational SecA states, largely via NBD2/γ-phosphate, and promote multiple, minor local dynamics changes. None of these significantly alter PBD motion (Figure S6E).

Preproteins regulate nucleotide-controlled dynamics in channel-bound SecA

How do preproteins exploit the nucleotide-regulated dynamics of the primed translocase leading to translocation? For this, we followed SecYEG:SecA$_2$:nucleotide dynamics (as in Figure 5A) with a bound secretory client (15 μM proPhoA$_{1\text{-}122}$; >50 fold over K_d; Figures 5B and S5D).

Motor dynamics with ADP were enhanced (Figures 5BI and S6C), due to preprotein-induced ADP release (Figure 1B). Compared to ADP, AMPPNP enhanced the dynamics in motifs I, Ic, III, and VI (Figures 5BII and S1E) and inside the clamp (3β-tip, β24$_{C\text{-}tail}$) and decreased them at the signal peptide binding cleft (stem, α10, α13). The contrasting dynamics flanking PBD suggested that ATP binding divergently affects the signal peptide and mature domain binding sites. ADP:BeF$_X$ reduced dynamics in all NBD2 helicase motifs without affecting NBD1 and rigidified clamp areas (stem, α13, 3β-tip, joint, scaffold; Figure 5BIII). These changes coincide with signal peptide-driven, nucleotide-independent clamp closing (Figure S3BIII). The preprotein coupled the otherwise unconnected nucleotide-regulated motor dynamics to clamp motions.

Nucleotides intimately regulate motor dynamics with minor effects on preprotein binding regions. However, clients not only

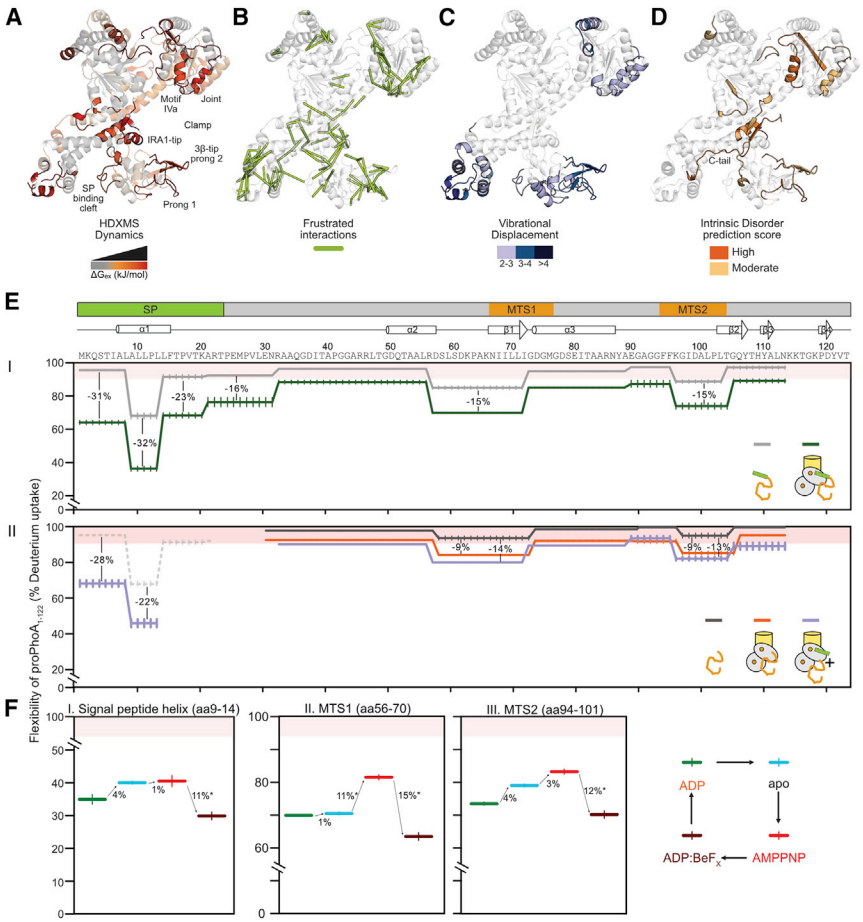

Figure 6. Translocase binds and regulates dynamics of preprotein islands

(A–D) Multi-parametric analysis of SecA flexibility mapped on *ec*SecA$_{2VDA}$ (open clamp; PDB:2VDA). C-tail from *ec*SecA$_{1M6N}$ (PDB:1M6N). (A) ΔG_{ex} values for SecA$_2$, red hues: high flexibility (i.e., ΔG_{ex} = 11–16 kJ/mol). (B) Frustrated regions (Frustratometer; Parra et al., 2016). (C) Total displacement of normal modes 7–12 (unweighted sum) (details in Figure S7C). (D) Predicted intrinsic disorder (MobiDB-lite aggregator; MobiDB database). Predictions/consensus: high/extensive multi tool (orange); moderate (Yellow).

(E) Flexibility map of free or translocase-bound proPhoA$_{1-122}$ (I) and PhoA$_{23-122}$ (II) as indicated (residue level absolute dynamics; percent D uptake), aligned below a linear map with signal peptide and MTS (mature domain targeting signals) 1 and 2 and known secondary structural features of native PhoA. Percent D uptake: >90%: hyper-flexible/disordered residues; 90–60%: increased flexibility. Purple: dynamics of PhoA$_{23-122}$ with signal peptide added *in trans*. Dashed gray: signal peptide flexibility in free proPhoA$_{1-122}$ (from I). Differences >10% are considered significant. n = *3*; SD values >1% are shown (vertical lines).

(F) Flexibility map of the indicated SecYEG: SecA$_2$:proPhoA$_{1-122}$ regions (with percent D uptake differences between states) as the translocase goes through the nucleotide cycle (right, as colored): ADP-ground state; ADP release (apo; light b), ATP bound (mimic: AMPPNP), and ATP hydrolysis transition state (mimic: ADP:BeF$_X$).

strengthen nucleotide effects at the motor, but they also cause nucleotide-modulated dynamics at multi-valent preprotein binding sites for successful translocation.

Locally frustrated prongs in the SecA clamp allow client promiscuity

The translocase handles hundreds of dissimilar clients presumably binding to the same SecA sites. For universal chaperone promiscuity, frustrated, dynamic elements in chaperones may recognize frustrated regions on non-folded clients (He et al., 2016; Hiller, 2019). Dynamic regions seen around the SecA clamp might exert similar mechanisms. To test this we compared the dynamic islands determined by HDX-MS (Figure 6A, orange/red) to frustrated predicted regions (Parra et al., 2016). Most frustrated inter-residue contacts (Figure 6B; green lines) closely overlap with the experimentally determined dynamic islands (Figure 6A). Clamp closing upon signal peptide binding (Figure 3A, lanes 7–12) would allow the 3β-tip, prong1, and joint to interact, forming a contiguous frustrated region (Figure S7AII) that could trap clients through local favorable interactions. In the ATP hydrolysis transition state (ADP:BeF$_X$; Figure S7B), two parallel regions of frustration and the closed clamp could enclose client chains during channel entry.

We further probed intrinsic dynamics in SecA's clamp using normal mode analysis (NMA), a mathematical description of atomic vibrational motions and protein flexibility (Bahar et al., 2010; Kovacs et al., 2004). The model generates a set of *normal modes*, where all Cα atoms are oscillating with the same frequency. The lowest frequency normal modes contribute the most to protein domain dynamics and the associated Cα displacement is calculated (Figure S7C; Hinsen, 1998; Tiwari et al., 2014). Motif IVa, Joint$_{NBD2}$, 3β-tip$_{PBD}$, and the signal peptide binding cleft show maximum displacement during vibrational motions (Figure 6C; blue shades) and practically coincide with the HDX-MS-determined dynamic islands and the frustrated regions. Finally, we tested the intrinsic disorder propensity of SecA using online predictors such as the MobiDB database (Piovesan et al., 2021). Several of the flexible regions identified by HDX-MS yield high predicted disorder scores (Figure 6D), eight of which (including in the PBD, NBD2, IRA1-tip, and the C-tail; Orange) were from a wide tool consensus.

Altered dynamics in the flexible prongs are subject to direct nucleotide modulation and promiscuous, local, rigidifying interactions with non-folded clients. These would couple client catch and release to the ATPase cycle.

Signal peptide-driven clamp closing enhances mature domain binding

Nucleotide-regulated motor or clamp dynamics allow for multivalent localized, transient interactions of non-folded clients with SecA. To probe how dynamics translate to client translocation steps, we monitored the dynamics of proPhoA$_{1\text{-}122}$ by HDX-MS (Figure S7D). This client contains three necessary and sufficient elements for translocase binding and secretion: a signal peptide and two mature domain targeting signals (MTS1-2; Figure 6E, top) (Chatzi et al., 2017).

In solution, proPhoA$_{1\text{-}122}$ is highly flexibile (Figure 6EI, gray), consistent with extensive non-foldedness (>90% D uptake; Figure 6EI, pink area) and lack of stable secondary structure (typically 20%–40% D uptake; Tsirigotaki et al., 2017b). Only three islands show some backbone stabilization signifying H bonding/transient acquisition of secondary structure (<90% D uptake): (1) the signal peptide hydrophobic core (aa 9–13) and ~17 residues downstream (Sardis et al., 2017), (2) the hydrophobic core (aa 68–72) and upstream more polar stretch (aa 56–68) of MTS1, and (3) the hydrophobic core of MTS2 (aa 94–102). The stabilized MTS1/2 regions overlap with natively folded PhoA secondary structures.

proPhoA$_{1\text{-}122}$ bound to SecYEG:SecA$_2$ shows significantly reduced D uptake (i.e., rigidification) in the signal peptide region (aa 1–33) and substantially in MTS1 and 2 (Figure 6EI, green line), while their connecting linkers remain highly unstructured (>85% D uptake). These rigidified islands reflect stabilized H bonds either within secondary structure elements or externally and are a direct demonstration of binding to SecA. Mature domain binding to SecYEG:SecA$_2$ exhibited less rigidification (Figure 6EII, compare black to orange and to Figure 6EI) that barely increased by *trans* addition of signal peptide (Figure 6EII, purple line) or use of SecY$_{PrlA4}$:SecA$_2$ (Figure S7E, purple), and it never reached that seen with preprotein. These data rationalize why preprotein moieties must be covalently connected for maximal translocase interaction.

The ATP cycle selectively alters SecA interaction with preprotein islands

To dissect how the ATPase cycle influences the dynamics of the islands of proPhoA$_{1\text{-}122}$ that bind SecA (Figures 6FI–6FIII), we monitored them in the four translocase:nucleotide analog conformations (Figure 6F, right).

When transitioning from the ADP-bound to the apoprotein to the AMPPNP-bound translocase, the signal peptide region shows slight rigidification and a significant one on the ADP:BeF$_X$-bound translocase (Figure 6FI, red to brown). MTS1 dynamics are unchanged when transitioning from the ADP-bound to the apo translocase but increase in the AMPPNP state (Figure 6FII, blue to red) and decrease in the ADP:BeF$_X$ state (red to brown). For MTS2, as the ATPase cycle progresses from ADP-bound to apo to AMPPNP state, its dynamics increase incrementally (Figure 6FIII, green to blue to red) but decrease significantly in the ADP:BeF$_X$ state (red to brown).

Our results suggest that SecA binds all three client elements in the ADP and apo states of a translocation cycle. ATP binding (mimic: AMPPNP) enhances SecA dynamics (Figure 5BII) and loosens its grip on the mature domain. The decreased dynamics of the signal peptide throughout the ATPase cycle (Figure 6FI) are consistent with the client remaining largely tethered to the translocase via its signal peptide, while mature domain parts associate or dissociate more dynamically (Burmann et al., 2013). During ATP hydrolysis transition, all client regions that bind SecA become rigidified (Figures 6FI–6FIII), likely reflecting tight trapping inside the ADP:BeF$_X$-driven rigidified closed-flipped clamp (Figure 5BIII). Upon ATP to ADP hydrolysis the translocase becomes more dynamic (Figure 5BIV) and modestly relaxes its grasp on the client (Figure 6F, brown to green). In this recreated ATP cycle, every translocase state has distinct "catch and release" consequences on each on the three client islands.

DISCUSSION

Gradual activation of the translocase involves hierarchical interactions (e.g., holoenzyme assembly, nucleotide or client binding), stemming from independent sub-reactions (e.g., clients bind either onto cytoplasmic or channel-primed SecA). How the Sec translocase or any nanomachine achieves hierarchical activation triggered promiscuously by hundreds of clients remains elusive. We reveal here a sophisticated two-part mechanism whereby various client-triggered interactions work in concert to activate translocase conformational switches and alter dynamics to ensure translocation.

Evolution prevented a readily activated SecA$_2$, favoring quiescence (Krishnamurthy et al., 2021). The translocase conformational ensemble becomes activated by regulating pre-existing subunit dynamics (Ahdash et al., 2019; Corey et al., 2019). The full compendium of pre-existing conformations arise from thermal atomic vibrations (Figures 6C and S7C) (Bahar et al., 2010; Chen and Komives, 2021; Dobbins et al., 2008; Smit et al., 2021c). These are differentially sampled over minor energetic barriers (Henzler-Wildman and Kern, 2007) tipped over by ligands (e.g., ATP, preproteins) that bias overpopulation of certain equilibrium states. These minor energetic requirements allow point mutations to mimic ligand binding effects (e.g., triggering, ATPase stimulation, enhanced dynamics) (Figure 2C) (Gouridis et al., 2009, 2013; Karamanou et al., 2007).

SecA bears two distinct modules, an ATPase hardwired onto a preprotein clamp (Figure 7I, gray), which assemble onto the channel (yellow). Both modules display distinct local and domain dynamics, largely uncoupled from each other and each finely controlled by a ligand. Non-folded clients couple the dynamics of the two modules. By binding to multiple SecA sites, clients physically bridge the modules, all the while tuning their dynamics (Figure 7II). Gate2 and stem control this coupling and regulate the transduction of conformational signals downstream, to effectuate enzymatic activation, first with ADP release (Figures 7III and 7IV), followed by fresh ATP binding (Figure 7V). The nucleotide state of the motor dictates the conformation of frustrated prongs in the clamp. As a result, the prongs catch and release the client chain, at multiple locations, biasing its forward motion (Figures 7III and 7VI).

Despite overall similarities between polypeptides, only secretory preproteins are legitimate translocase clients. Alone, signal peptides and mature domains alter distinctly but partially the

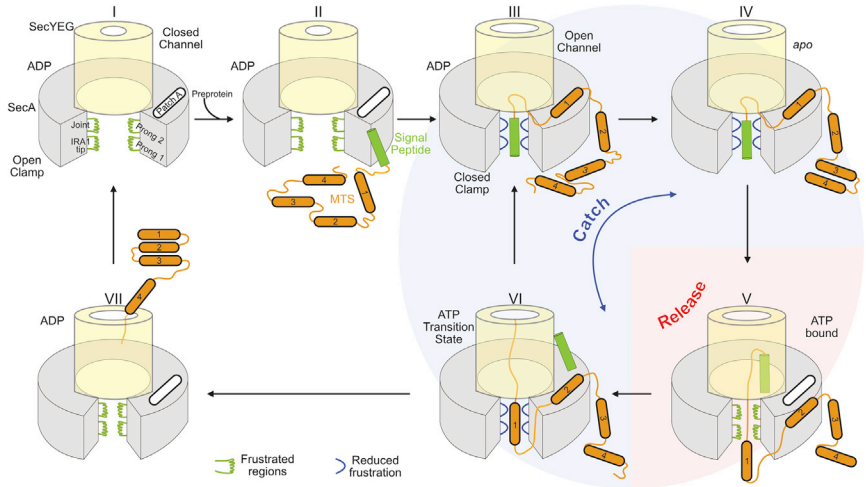

Figure 7. Catch and release model for preprotein translocation

See text for details. Green: enhanced and blue: reduced frustrated regions. PatchA: MTS binding site.

dynamics of the switches, with inadequate functional effects (Figures 3 and 4). Signal peptides close the clamp (Figure 3A, lanes 10–12), partially elevate gate2 dynamics (Figures 2A and 2B), and loosen the channel (Figures 7II and 7III) (Fessl et al., 2018; Knyazev et al., 2014). Mature domains partially increase the motor's dynamics (Figure S4G) and drive inefficient ADP release (Figure 4D). It is the synergy between the two covalently connected moieties that secures adequate motor dynamics for ADP release (Figures 1B, 1CII, and 1CIII), a key rate limiting step (Fak et al., 2004; Robson et al., 2009; Sianidis et al., 2001). This mechanism expels random cytoplasmic proteins from secretion.

ATP binding to the motor initiates translocation (Figure 7V). As the translocase cycles through nucleotide states it manipulates the client's dynamics. The ATP-bound translocase binds signal peptides, releasing mature domain segments (Figure 6E, red). In the transition state it *catches* both signal peptide and mature domain targeting signals (MTS) regions (Figures 5BIII and 6B and 6E). In the ADP-bound state, a succeeding region from the bound client will induce ADP release (Figure 1B) to restart an ATP hydrolysis cycle. Cycles repeat for as long as succeeding mature domain segments are available to bind to the translocase and drive ADP release (Figures 7III–7VI). In their absence, SecA:ADP remains quiescent, diffuses to the cytoplasmic pool, and dimerizes (Gouridis et al., 2013). Secretion is achieved through such repetitive client catch and release cycles regulated by nucleotide turnovers (Figure 7). The mechanism is generic for initial as well as subsequent processive translocation steps (Figure 1AV). Later in translocation, cleaved signal peptides are replaced by hydrophobic MTSs (Chatzi et al., 2017) (Figure 7VI).

SecA dynamics sense the slightest chemical change in nucleotides and invite a rethink of the role of ATP hydrolysis in translocation. Rather than driving major deterministic strokes, nucleotides subtly, stepwise, bias SecA's intrinsic dynamics (Figure 5) by affecting residues that line the nucleotide cleft. The limited, transient interaction of the γ-phosphate of ATP and its transition states with NBD2 bias motor conformational cycles, which stop when it is absent (Figures 1B and 7I–7VI) (Keramisanou et al., 2006; Papanikolau et al., 2007; Sianidis et al., 2001).

An underappreciated feature of secretory clients is their elevated intrinsic dynamics, which when reduced, abrogated secretion (Sardis et al., 2017). HDX-MS uniquely captured islands of dynamics in the secretory chain (e.g., signal peptide, early mature domain, and MTSs) (Figures 6EI and 7II) (Sardis et al., 2017) that respond to the transient, nucleotide states of the translocase (Figure 6E). How does SecA, a weak cytoplasmic and strong membrane-associated holdase (Gouridis et al., 2009), promiscuously recognize its clients? Chaperones may recognize frustrated regions in clients through their own frustrated regions (He and Hiller, 2019; Hiller, 2019), as does SecA (Figure 6B). Client's or chaperone's frustrated regions can sample a wide conformational and sequence space, until they interact tightly (Ferreiro et al., 2014; He and Hiller, 2018). Thus, a chaperone can promiscuously interact with hundreds of non-folded clients without rigid lock-and-key recognition. In SecA, the four highly dynamic, locally frustrated prongs around the clamp (Figures 6A and 6B and 7I–7III), the electronegativity of the clamp (Figure S5B), and its adjustable width due to PBD/NBD2 rigid body motions enhance plasticity and interactions, potentially accommodating partially folded structures (Tsirigotaki et al., 2018). Client-translocase interactions reduce dynamics both in the frustrated SecA prongs (Figures 5BIII and 7, green) and the corresponding frustrated elements of the client (Figure 6E). Such a mechanism permits high affinity yet transient interactions with the client and fast release, formulating an optimal solution for secretion. Tighter recognition of unfolded clients might have impeded SecA's processivity.

SecA biases vectorial forward motion, uncommon in soluble chaperones. Presumably, local interactions of frustrated prongs are sufficient to stall backward sliding of the exported chain yet loose enough to allow forward motion of untethered segments through the channel. This *catch and release* mechanism is important for translocation. Release cycles allow chain segments to enter the channel by Brownian motion (Allen et al., 2016) catch cycles would bind a downstream segment and prevent back-slippage (Figures 7V and 7VI), like a ''brake'' (Vandenberk et al., 2019). This mechanism is also compatible with a power stroke, if *catching* actively carries along chain segments into the channel (Catipovic et al., 2019) or with a continuum ratchet, SecA moving stochastically along a periodic potential, coupled to ATP cycling, providing the required time correlation for net vectorial motion (Magnasco, 1993). All models depend on *catch* signals like MTSs (Figures 6E and 6F).

A short preprotein with limited folding permitted dissection of translocase binding from folding propensities but the same fundamental principles revealed likely apply to longer clients. Most secretory proteins are flexible with delayed folding but some may rapidly fold (Arkowitz et al., 1993; Gupta et al., 2020; Tsirigotaki et al., 2018). Translocase dynamics may counter such inherent folding forces alone, or in concert with chaperones (De Geyter et al., 2020; Fekkes et al., 1997).

Limitations of the study

$SecA_2$ binds asymmetrically to SecYEG, using one of its protomers. $SecA_2$ is essential to initiate translocation, but later monomerizes. The ensemble nature of HDX-MS cannot delineate the differences in dynamics between the two protomers. This will require immobilized single-molecule techniques.

Here, we monitored client protein dynamics using ATP analogs that are assumed to mimic distinct stages of the nucleotide cycle during translocation. These analogs may not accurately represent stages in the ATP hydrolysis cycle, therefore weakening our interpretation. Furthermore, to synchronize ATP-dependent translocation of all clients in the ensemble and follow their dynamics by HDX-MS during processive translocation remains challenging and is not explored in this study.

This study monitored translocation steps using the minimal functional translocase SecYEG:$SecA_2$ and a single preprotein. The model we present here may not fully explain *in vivo* delivery and secretion of multiple preproteins from the ribosome to the translocase that involves chaperones and feedback mechanisms.

STAR★METHODS

Detailed methods are provided in the online version of this paper and include the following:

- KEY RESOURCES TABLE
- RESOURCE AVAILABILITY
  - Lead contact
  - Materials availability
  - Data and code availability
- EXPERIMENTAL MODEL AND SUBJECT DETAILS
- METHOD DETAILS
  - List of buffers
  - Molecular cloning
  - Protein purification
  - MANT-ADP release assays
  - Dynamics of the Sec translocase by HDX-MS
  - HDX-MS data visualization
  - Dynamics of client proteins by HDX-MS
  - Determination of ΔG_{ex} values
  - Single-molecule fluorescence microscopy and PIE
  - H-bonding graph analysis
  - Normal mode analysis and intrinsic disorder prediction
  - Miscellaneous
- QUANTIFICATION AND STATISTICAL ANALYSIS
  - MANT-ADP release assays
  - HDX-MS data
  - Biochemical assays
  - smFRET data

SUPPLEMENTAL INFORMATION

Supplemental information can be found online at https://doi.org/10.1016/j.celrep.2022.110346.

ACKNOWLEDGMENTS

We are grateful to: T. Cordes for sharing software for smFRET data analysis. Our research was funded by grants (to AE): MeNaGe (RUN #RUN/16/001; KU Leuven); ProFlow (FWO/F.R.S. - FNRS "Excellence of Science - EOS" program grant #30550343); DIP-BiD (#AKUL/15/40 - G0H2116N; Hercules/FWO); CARBS (#G0C6814N; FWO); Profound (WoG Research Training Network, FWO, Protein folding/non-folding and dynamics; #W002421N) and (to AE and SK): FOscil (ZKD4582-C16/18/008; KU Leuven) and (to A-NB): by the Excellence Initiative of the German Federal and State Governments via the Freie Universität Berlin, and by allocations of computing time from the North-German Supercomputing Alliance, HLRN. S.Kr. was an FWO [PEGASUS]^2 MSC fellow; N.E. was an MSCA SoE FWO fellow; J.H.S. is a PDM/KU Leuven fellow; G.G. was a Rega Foundation postdoctoral program fellow. This project has received funding from the Research Foundation Flanders (FWO) and the European Union's Horizon 2020 research and innovation program under the Marie Skłodowska-Curie grant agreements No. 665501 and 195872.

AUTHOR CONTRIBUTIONS

S.Kr. purified proteins and membranes, did biochemical and fluorescence assays, designed and performed HDX-MS work and data analysis. M.F.S. and K.E.C. purified proteins, performed molecular biology, *in vivo* and *in vitro* biochemical and biophysical assays. N.E. purified and labeled proteins and performed smFRET experiments and data analysis. J.H.S. developed PyHDX software and analyzed HDX-MS data, adapted FRET burst analysis for Microtime200 output data, and performed NMA analysis. K.K. performed MD simulations and graph analysis of H bond networks. G.G. performed biochemical, molecular biology, and biophysical assays, analyzed data and advised on smFRET. A.G.P. performed molecular cloning and mutagenesis. A.N.B. set up and supervised the MD simulations and graph analysis. S.K. designed and supervised molecular biology experiments, purified proteins, performed biochemical and biophysical assays and data analysis. A.E. did structure and data analysis and designed experiments. S.Kr. and A.E. wrote the first draft and finalized it with contributions from S.K., A.N.B., J.H.S., and N.E. All authors reviewed and approved the final manuscript. A.E. and S.K. conceived and managed the project.

DECLARATION OF INTERESTS

The authors declare no competing interests.

Received: August 31, 2021
Revised: November 22, 2021
Accepted: January 12, 2022
Published: February 8, 2022

SUPPORTING CITATIONS

The following reference appears in the Supplemental information: Baker et al., 2001; Lacabanne et al., 2020.

REFERENCES

Ahdash, Z., Pyle, E., Allen, W.J., Corey, R.A., Collinson, I., and Politis, A. (2019). HDX-MS reveals nucleotide-dependent, anti-correlated opening and closure of SecA and SecY channels of the bacterial translocon. Elife *8*, e47402.

Allen, W.J., Corey, R.A., Oatley, P., Sessions, R.B., Baldwin, S.A., Radford, S.E., Tuma, R., and Collinson, I. (2016). Two-way communication between

SecY and SecA suggests a Brownian ratchet mechanism for protein translocation. Elife *5*, e15598.

Arkowitz, R.A., Joly, J.C., and Wickner, W. (1993). Translocation can drive the unfolding of a preprotein domain. EMBO J. *12*, 243–253.

Avellaneda, M.J., Koers, E.J., Naqvi, M.M., and Tans, S.J. (2017). The chaperone toolbox at the single-molecule level: from clamping to confining. Protein Sci. *26*, 1291–1302.

Bahar, I., Lezon, T.R., Bakan, A., and Shrivastava, I.H. (2010). Normal mode analysis of biomolecular structures: functional mechanisms of membrane proteins. Chem. Rev. *110*, 1463–1497.

Baker, N.A., Sept, D., Joseph, S., Holst, M.J., and McCammon, J.A. (2001). Electrostatics of nanosystems: application to microtubules and the ribosome. Proc. Natl. Acad. Sci. U.S.A *98*, 10037–10041.

Bauer, B.W., and Rapoport, T.A. (2009). Mapping polypeptide interactions of the SecA ATPase during translocation. Proc. Natl. Acad. Sci. U.S.A *106*, 20800–20805.

Burmann, B.M., Wang, C., and Hiller, S. (2013). Conformation and dynamics of the periplasmic membrane-protein-chaperone complexes OmpX-Skp and tOmpA-Skp. Nat. Struct. Mol. Biol. *20*, 1265–1272.

Catipovic, M.A., Bauer, B.W., Loparo, J.J., and Rapoport, T.A. (2019). Protein translocation by the SecA ATPase occurs by a power-stroke mechanism. EMBO J. *38*, e101140.

Chatzi, K.I., Gouridis, G., Orfanoudaki, G., Koukaki, M., Tsamardinos, I., Karamanou, S., and Economou, A. (2011). The signal peptides and the early mature domain cooperate for efficient secretion. FEBS J. *278*, 14.

Chatzi, K.E., Sardis, M.F., Tsirigotaki, A., Koukaki, M., Sostaric, N., Konijnenberg, A., Sobott, F., Kalodimos, C.G., Karamanou, S., and Economou, A. (2017). Preprotein mature domains contain translocase targeting signals that are essential for secretion. J. Cel. Biol. *216*, 1357–1369.

Chen, W., and Komives, E.A. (2021). Open, engage, bind, translocate: the multi-level dynamics of bacterial protein translocation. Structure *29*, 781–782.

Corey, R.A., Ahdash, Z., Shah, A., Pyle, E., Allen, W.J., Fessl, T., Lovett, J.E., Politis, A., and Collinson, I. (2019). ATP-induced asymmetric pre-protein folding as a driver of protein translocation through the Sec machinery. Elife *8*, e41803.

Cryar, A., Groves, K., and Quaglia, M. (2017). Online hydrogen-deuterium exchange traveling wave ion mobility mass spectrometry (HDX-IM-MS): a systematic evaluation. J. Am. Soc. Mass Spectrom. *28*, 1192–1202.

De Geyter, J., Portaliou, A.G., Srinivasu, B., Krishnamurthy, S., Economou, A., and Karamanou, S. (2020). Trigger factor is a bona fide secretory pathway chaperone that interacts with SecB and the translocase. EMBO Rep. *21*, e49054.

Dobbins, S.E., Lesk, V.I., and Sternberg, M.J. (2008). Insights into protein flexibility: the relationship between normal modes and conformational change upon protein-protein docking. Proc. Natl. Acad. Sci. U S A *105*, 10390–10395.

Dunker, A.K., Brown, C.J., Lawson, J.D., Iakoucheva, L.M., and Obradovic, Z. (2002). Intrinsic disorder and protein function. Biochemistry *41*, 6573–6582.

Erdos, G., Pajkos, M., and Dosztanyi, Z. (2021). IUPred3: prediction of protein disorder enhanced with unambiguous experimental annotation and visualization of evolutionary conservation. Nucleic Acids Res. *49*, W297–W303.

Ernst, I., Haase, M., Ernst, S., Yuan, S., Kuhn, A., and Leptihn, S. (2018). Large conformational changes of a highly dynamic pre-protein binding domain in SecA. Commun. Biol. *1*, 130.

Fak, J.J., Itkin, A., Ciobanu, D.D., Lin, E.C., Song, X.J., Chou, Y.T., Gierasch, L.M., and Hunt, J.F. (2004). Nucleotide exchange from the high-affinity ATP-binding site in SecA is the rate-limiting step in the ATPase cycle of the soluble enzyme and occurs through a specialized conformational state. Biochemistry *43*, 7307–7327.

Fekkes, P., van der Does, C., and Driessen, A.J. (1997). The molecular chaperone SecB is released from the carboxy-terminus of SecA during initiation of precursor protein translocation. EMBO J. *16*, 6105–6113.

Ferreiro, D.U., Komives, E.A., and Wolynes, P.G. (2014). Frustration in biomolecules. Q. Rev. Biophys. *47*, 285–363.

Fessl, T., Watkins, D., Oatley, P., Allen, W.J., Corey, R.A., Horne, J., Baldwin, S.A., Radford, S.E., Collinson, I., and Tuma, R. (2018). Dynamic action of the Sec machinery during initiation, protein translocation and termination. Elife *7*, e35112.

Flechsig, H., and Mikhailov, A.S. (2019). Simple mechanics of protein machines. J. R. Soc. Interf. *16*, 20190244.

Flower, A.M., Doebele, R.C., and Silhavy, T.J. (1994). PrlA and PrlG suppressors reduce the requirement for signal sequence recognition. J. Bacteriol. *176*, 5607–5614.

Fuxreiter, M., Toth-Petroczy, A., Kraut, D.A., Matouschek, A., Lim, R.Y., Xue, B., Kurgan, L., and Uversky, V.N. (2014). Disordered proteinaceous machines. Chem. Rev. *114*, 6806–6843.

Galletto, R., Jezewska, M.J., Maillard, R., and Bujalowski, W. (2005). The nucleotide-binding site of the *Escherichia coli* DnaC protein: molecular topography of DnaC protein-nucleotide cofactor complexes. Cell Biochem. Biophys. *43*, 331–353.

Gelis, I., Bonvin, A.M., Keramisanou, D., Koukaki, M., Gouridis, G., Karamanou, S., Economou, A., and Kalodimos, C.G. (2007). Structural basis for signal-sequence recognition by the translocase motor SecA as determined by NMR. Cell *131*, 756–769.

Gouridis, G., Karamanou, S., Gelis, I., Kalodimos, C.G., and Economou, A. (2009). Signal peptides are allosteric activators of the protein translocase. Nature *462*, 363–367.

Gouridis, G., Karamanou, S., Koukaki, M., and Economou, A. (2010). In vitro assays to analyze translocation of the model secretory preprotein alkaline phosphatase. Methods Mol. Biol. *619*, 157–172.

Gouridis, G., Karamanou, S., Sardis, M.F., Scharer, M.A., Capitani, G., and Economou, A. (2013). Quaternary dynamics of the SecA motor drive translocase catalysis. Mol. Cell *52*, 655–666.

Gupta, R., Toptygin, D., and Kaiser, C.M. (2020). The SecA motor generates mechanical force during protein translocation. Nat. Commun. *11*, 3802.

Hanson, J., Yang, Y., Paliwal, K., and Zhou, Y. (2017). Improving protein disorder prediction by deep bidirectional long short-term memory recurrent neural networks. Bioinformatics *33*, 685–692.

Hartl, F.U., Lecker, S., Schiebel, E., Hendrick, J.P., and Wickner, W. (1990). The binding cascade of SecB to SecA to SecY/E mediates preprotein targeting to the *E. coli* plasma membrane. Cell *63*, 269–279.

He, L., and Hiller, S. (2018). Common patterns in chaperone interactions with a native client protein. Angew. Chem. Int. Ed. Engl. *57*, 5921–5924.

He, L., and Hiller, S. (2019). Frustrated interfaces facilitate dynamic interactions between native client proteins and holdase chaperones. Chembiochem *20*, 2803–2806.

He, L., Sharpe, T., Mazur, A., and Hiller, S. (2016). A molecular mechanism of chaperone-client recognition. Sci. Adv. *2*, e1601625.

Henzler-Wildman, K., and Kern, D. (2007). Dynamic personalities of proteins. Nature *450*, 964–972.

Henzler-Wildman, K.A., Lei, M., Thai, V., Kerns, S.J., Karplus, M., and Kern, D. (2007). A hierarchy of timescales in protein dynamics is linked to enzyme catalysis. Nature *450*, 913–916.

Hiller, S. (2019). Chaperone-bound clients: the importance of being dynamic. Trends Biochem. Sci. *44*, 517–527.

Hinsen, K. (1998). Analysis of domain motions by approximate normal mode calculations. Proteins *33*, 417–429.

Houde, D., Berkowitz, S.A., and Engen, J.R. (2011). The utility of hydrogen/deuterium exchange mass spectrometry in biopharmaceutical comparability studies. J. Pharm. Sci. *100*, 2071–2086.

Hu, G., Katuwawala, A., Wang, K., Wu, Z., Ghadermarzi, S., Gao, J., and Kurgan, L. (2021). flDPnn: accurate intrinsic disorder prediction with putative propensities of disorder functions. Nat. Commun. *12*, 4438.

Huie, J.L., and Silhavy, T.J. (1995). Suppression of signal sequence defects and azide resistance in *Escherichia coli* commonly result from the same mutations in secA. J. Bacteriol. *177*, 3518–3526.

Karamanou, S., Sianidis, G., Gouridis, G., Pozidis, C., Papanikolau, Y., Papanikou, E., and Economou, A. (2005). *Escherichia coli* SecA truncated at its termini is functional and dimeric. FEBS Lett. *579*, 1267–1271.

Karamanou, S., Gouridis, G., Papanikou, E., Sianidis, G., Gelis, I., Keramisanou, D., Vrontou, E., Kalodimos, C.G., and Economou, A. (2007). Preprotein-controlled catalysis in the helicase motor of SecA. EMBO J. *26*, 2904–2914.

Karathanou, K., and Bondar, A.N. (2019). Using graphs of dynamic hydrogen-bond networks to dissect conformational coupling in a protein motor. J. Chem. Inf. Model. *59*, 1882–1896.

Keramisanou, D., Biris, N., Gelis, I., Sianidis, G., Karamanou, S., Economou, A., and Kalodimos, C.G. (2006). Disorder-order folding transitions underlie catalysis in the helicase motor of SecA. Nat. Struct. Mol. Biol. *13*, 594–602.

Knyazev, D.G., Winter, L., Bauer, B.W., Siligan, C., and Pohl, P. (2014). Ion conductivity of the bacterial translocation channel SecYEG engaged in translocation. J. Biol. Chem. *289*, 24611–24616.

Kovacs, J.A., Chacon, P., and Abagyan, R. (2004). Predictions of protein flexibility: first-order measures. Proteins *56*, 661–668.

Krishnamurthy, S., Eleftheriadis, N., Karathanou, K., Smit, J.H., Portaliou, A.G., Chatzi, K.E., Karamanou, S., Bondar, A.N., Gouridis, G., and Economou, A. (2021). A nexus of intrinsic dynamics underlies translocase priming. Structure *29*, 846–858 e847.

Kurakin, A. (2006). Self-organization versus watchmaker: molecular motors and protein translocation. Biosystems *84*, 15–23.

Lacabanne, D., Wiegand, T., Wili, N., Kozlova, M.I., Cadalbert, R., Klose, D., Mulkidjanian, A.Y., Meier, B.H., and Bockmann, A. (2020). ATP analogues for structural investigations: case studies of a DnaB helicase and an ABC transporter. Molecules *25*, 5268.

Lill, R., Cunningham, K., Brundage, L.A., Ito, K., Oliver, D., and Wickner, W. (1989). SecA protein hydrolyzes ATP and is an essential component of the protein translocation ATPase of *Escherichia coli*. EMBO J. *8*, 961–966.

Lill, R., Dowhan, W., and Wickner, W. (1990). The ATPase activity of SecA is regulated by acidic phospholipids, SecY, and the leader and mature domains of precursor proteins. Cell *60*, 271–280.

Linding, R., Jensen, L.J., Diella, F., Bork, P., Gibson, T.J., and Russell, R.B. (2003). Protein disorder prediction: implications for structural proteomics. Structure *11*, 1453–1459.

Loutchko, D., and Flechsig, H. (2020). Allosteric communication in molecular machines via information exchange: what can be learned from dynamical modeling. Biophys. Rev. *15*, 443–452.

Magnasco, M.O. (1993). Forced thermal ratchets. Phys. Rev. Lett. *71*, 1477–1481.

Mitchell, C., and Oliver, D. (1993). Two distinct ATP-binding domains are needed to promote protein export by *Escherichia coli* SecA ATPase. Mol. Microbiol. *10*, 483–497.

Nussinov, R., Zhang, M., Tsai, C.J., Liao, T.J., Fushman, D., and Jang, H. (2018). Autoinhibition in Ras effectors Raf, PI3Kalpha, and RASSF5: a comprehensive review underscoring the challenges in pharmacological intervention. Biophys. Rev. *10*, 1263–1282.

Or, E., Navon, A., and Rapoport, T. (2002). Dissociation of the dimeric SecA ATPase during protein translocation across the bacterial membrane. EMBO J. *21*, 4470–4479.

Papanikolau, Y., Papadovasilaki, M., Ravelli, R.B., McCarthy, A.A., Cusack, S., Economou, A., and Petratos, K. (2007). Structure of dimeric SecA, the *Escherichia coli* preprotein translocase motor. J. Mol. Biol. *366*, 1545–1557.

Parra, R.G., Schafer, N.P., Radusky, L.G., Tsai, M.Y., Guzovsky, A.B., Wolynes, P.G., and Ferreiro, D.U. (2016). Protein Frustratometer 2: a tool to localize energetic frustration in protein molecules, now with electrostatics. Nucleic Acids Res. *44*, W356–W360.

Peng, K., Vucetic, S., Radivojac, P., Brown, C.J., Dunker, A.K., and Obradovic, Z. (2005). Optimizing long intrinsic disorder predictors with protein evolutionary information. J. Bioinform Comput. Biol. *3*, 35–60.

Piovesan, D., Necci, M., Escobedo, N., Monzon, A.M., Hatos, A., Micetic, I., Quaglia, F., Paladin, L., Ramasamy, P., Dosztanyi, Z., et al. (2021). MobiDB: intrinsically disordered proteins in 2021. Nucleic Acids Res. *49*, D361–D367.

Rapoport, T.A., Li, L., and Park, E. (2017). Structural and mechanistic insights into protein translocation. Annu. Rev. Cell Dev. Biol. *33*, 369–390.

Robson, A., Gold, V.A., Hodson, S., Clarke, A.R., and Collinson, I. (2009). Energy transduction in protein transport and the ATP hydrolytic cycle of SecA. Proc. Natl. Acad. Sci. U.S.A. *106*, 5111–5116.

Sardis, M.F., and Economou, A. (2010). SecA: a tale of two protomers. Mol. Microbiol. *76*, 1070–1081.

Sardis, M.F., Tsirigotaki, A., Chatzi, K.E., Portaliou, A.G., Gouridis, G., Karamanou, S., and Economou, A. (2017). Preprotein conformational dynamics drive bivalent translocase docking and secretion. Structure *25*, 1056–1067.e1056.

Sianidis, G., Karamanou, S., Vrontou, E., Boulias, K., Repanas, K., Kyrpides, N., Politou, A.S., and Economou, A. (2001). Cross-talk between catalytic and regulatory elements in a DEAD motor domain is essential for SecA function. EMBO J. *20*, 961–970.

Smit, J.H., Krishnamurthy, S., Srinivasu, B.Y., Parakra, R., Karamanou, S., and Economou, A. (2021a). Probing universal protein dynamics using hydrogen-deuterium exchange mass spectrometry-derived residue-level Gibbs free energy. Anal. Chem. *93*, 12840–12847.

Smit, J.H., Krishnamurthy, S., Srinivasu, B.Y., Parakra, R., Karamanou, S., and Economou, A. (2021b). Probing universal protein dynamics using residue-level Gibbs free energy. bioRxiv. https://doi.org/10.1101/2020.2009.2030.320887.

Smit, J.H., Roussel, G., and Economou, A. (2021c). Dynamics ante portas. Proc. Natl. Acad. Sci. U S A *118*, e2110553118.

Studier, F.W., Rosenberg, A.H., Dunn, J.J., and Dubendorff, J.W. (1990). Use of T7 RNA polymerase to direct expression of cloned genes. Methods Enzymol. *185*, 60–89.

Tiwari, S.P., Fuglebakk, E., Hollup, S.M., Skjaerven, L., Cragnolini, T., Grindhaug, S.H., Tekle, K.M., and Reuter, N. (2014). WEBnm@ v2.0: web server and services for comparing protein flexibility. BMC Bioinformatics *15*, 427.

Tsirigotaki, A., De Geyter, J., Sostaric, N., Economou, A., and Karamanou, S. (2017a). Protein export through the bacterial Sec pathway. Nat. Rev. Microbiol. *15*, 21–36.

Tsirigotaki, A., Papanastasiou, M., Trelle, M.B., Jorgensen, T.J., and Economou, A. (2017b). Analysis of translocation-competent secretory proteins by HDX-MS. Methods Enzymol. *586*, 57–83.

Tsirigotaki, A., Chatzi, K.E., Koukaki, M., De Geyter, J., Portaliou, A.G., Orfanoudaki, G., Sardis, M.F., Trelle, M.B., Jorgensen, T.J.D., Karamanou, S., et al. (2018). Long-lived folding intermediates predominate the targeting-competent secretome. Structure *26*, 695–707 e695.

Vandenberk, N., Karamanou, S., Portaliou, A.G., Zorzini, V., Hofkens, J., Hendrix, J., and Economou, A. (2019). The preprotein binding domain of SecA displays intrinsic rotational dynamics. Structure *27*, 90–101 e106.

Yang, L.Q., Sang, P., Tao, Y., Fu, Y.X., Zhang, K.Q., Xie, Y.H., and Liu, S.Q. (2014). Protein dynamics and motions in relation to their functions: several case studies and the underlying mechanisms. J. Biomol. Struct. Dyn. *32*, 372–393.

Zhang, Y., Doruker, P., Kaynak, B., Zhang, S., Krieger, J., Li, H., and Bahar, I. (2019). Intrinsic dynamics is evolutionarily optimized to enable allosteric behavior. Curr. Opin. Struct. Biol. *62*, 14–21.

Zimmer, J., Nam, Y., and Rapoport, T.A. (2008). Structure of a complex of the ATPase SecA and the protein-translocation channel. Nature *455*, 936–943.

STAR★METHODS

KEY RESOURCES TABLE

REAGENT or RESOURCE	SOURCE	IDENTIFIER
Bacterial and virus strains		
DH5α: *F– endA1 glnV44 thi-1 recA1 relA1 gyrA96 deoR nupG purB20 φ80dlacZΔM15 Δ(lacZYA-argF)U169, hsdR17(rK–mK+), λ–*	Invitrogen	Cat# 18258012
BL21 (DE3): T7 RNA polymerase gene under the control of the *lac* UV5 promoter	(Studier et al., 1990)	N/A
BL21.19 (DE3): *secA13(Am) clpA::kan, ts* at 42°C;	(Mitchell and Oliver, 1993)	N/A
BL31 (DE3): Non *ts*; spontaneous revertant of BL21.19 (DE3)	(Chatzi et al., 2017)	N/A
T7 Express lysY/I^q Competent *E. coli* (High Efficiency)	New England Biolabs	Cat# C3013I
Chemicals, peptides, and recombinant proteins		
Tris base	Sigma-Aldrich	Cat# T1378
NaCl	Sigma-Aldrich	Cat# 7647-14-5
Magnesium Chloride ($MgCl_2$)	Roth	Cat# 2189
Zinc Sulphate heptahydrate ($ZnSO_4$)	Roth	Cat# 7316.1
Ethylenediaminetetraaceticacid, diNa salt, 2aq (EDTA)	ChemLab	Cat# CL00.0503
Phenylmethylsulfonylfluoride (PMSF)	Roth	Cat# 6367
Dithiothreitol (DTT)	ApplichemPanreac	Cat# A1101
Cibacrom Blue 3GA	Sigma-Aldrich	Cat# B1064
proPhoA signal peptide lyophilized powder	Genscript	N/A
Trolox	Sigma-Aldrich	Cat# 53188-07-1
Alexa Fluor 555 C_2 Maleimide	Thermo Fisher Scientific	Cat# A20346
Alexa Fluor 647 C_2 Maleimide	Thermo Fisher Scientific	Cat# A20347
ADP (Adenosine 5′-Diphosphate)	Sigma-Aldrich	Cat# A2754
$BeCl_2$	American Elements	Cat# BE-CL-02M-C
NaF	Sigma-Aldrich	Cat# 450022
MANT-ADP (2′- (or-3′) - O - (N -Methylanthraniloyl) Adenosine 5′-Diphosphate, Disodium Salt)	Invitrogen/Thermo Fisher Scientific	Cat# M12416
TCEP ([Tris(2-carboxyethyl)phosphine]	Sigma-Aldrich	Cat# 51805-45-9
Bio-Rad Protein assay dye reagent	Bio-Rad	Cat# 5000006
Urea-d4 (98% D)	Sigma	Cat# 176087
Formic Acid (Ultra-pure)	Sigma-Aldrich	Cat# 330020050
PFU Ultra Polymerase	Promega	Cat# M7741
Dpn1	Promega	Cat# R6231
NdeI	Promega	Cat# R6801
BamHI	Promega	Cat# R6021
Acetonitrile	Merck Millipore	Cat#1000291000
Fungal protease type XIII	Sigma-Aldrich	Cat# P2143
Immobilized pepsin resin	Thermo Fisher Scientific	Cat# 20343
Deuterium Oxide (99.9%)	Euroisotop	Cat# D216

(*Continued on next page*)

Continued

REAGENT or RESOURCE	SOURCE	IDENTIFIER
Critical commercial assays		
QuickChange Site-directed mutagenesis protocol	Strategene-Agilent	N/A
Plasmid purification (NucleoSpin® Plasmid EasyPure)	Macherey- Nagel	Cat# 740727
Deposited data		
Crystal structure of ADP-bound dimeric SecA from *Escherichia coli*	(Papanikolau et al., 2007)	PDB: 2FSI
Model of monomeric *Escherichia coli* SecA with Closed clamp derived from MD simulations of PDB: 2VDA as starting structure.	(Krishnamurthy et al., 2021)	N/A
Model of the *E. coli* SecA:SecYEG complex proteins derived from the crystal structure of SecA:SecYEG complex from *T. maritima*.	(Zimmer et al., 2008) (Vandenberk et al., 2019)	PDB: 3DIN
Crystal structure of *Escherichia coli* SecA-signal peptide complex	(Gelis et al., 2007)	PDB: 2VDA
Oligonucleotides		
#	**Description**	**DNA sequence (5′-3′; Mutated codons in bold; restriction sites underlined)**
X182	Reverse *secA* primer for mega-primer mutagenesis	GGCCTTTCGCAGTACGTTC
X395	Forward primer to amplify from position 4190 to 4214 of pIMBB7 for mega-primer mutagenesis	CTAACAACAATAAACCTTTACTTC
X400	Reverse mutagenic primer for SecA(E181A)	GTCAAAGCCGTA**TGC**GTTGTTCGT
X401	Reverse mutagenic primer to generate *secA*(F184A)	GCGCAGGTAGTC**GGC**GCCGT ATTCGTTGTT
X402	Reverse mutagenic primer to generate *secA*(D185A)	GTCGCGCAGGTA**GGC**AAAGC CGTATTCGTTGTT
X403	Reverse mutagenic primer to generate *secA*(L187A)	CATGTTGTCGCG**CGC**GTAGTC AAAGCCGTA
X404	Reverse mutagenic primer to generate *secA*(R188A)	CATGTTGTC**GGC**CAGGTAGTCAAA
X405	Reverse mutagenic primer to generate *secA*(D189A)	GAACGCCATGTT**CGC**GCGCAGGT AGTCAAA
X406	Reverse mutagenic primer to generate *secA*(M191A)	CAGGGCTGAACGC**CGC**GTTGTCGCG
X409	Forward mutagenic primer to generate *secA*(A373V)	GAAAACCAAACGCTG**GTT**TCGATCAC
X423	Forward mutagenic primer generate *secA*(T340A/G341A/R342A)	GACGAACAC**GCCGCTGCT**ACCATG CAGGG
X560	Forward phoA primer introducing an NdeI restriction site	GGGAATTCCATATAAACAAAGC ACTATTGCA
X634	Forward mutagenic primer to generate *secA*(A373F)	GAAAACCAAACGCTG**TTT**TCGATCA CCTTCCAG
X635	Reverse mutagenic primer to generate *secA*(A373F)	CTGGAAGGTGATCGAAAACAGCGT TTGGTTTTC
X636	Forward mutagenic primer to generate *secA*(A373I)	GAAAACCAAACGCTGATTTCGAT CACCTTCCAG
X637	Reverse mutagenic primer to generate *secA*(A373I)	CTGGAAGGTGATCGAAATCAGCGTTTGG TTTTC
X638	Forward mutagenic primer to generate *secA*(L187V)	TACGGCTTTGACTACGTGCGCGAC AACATGGCG

(*Continued on next page*)

Continued

REAGENT or RESOURCE	SOURCE	IDENTIFIER
X639	Reverse mutagenic primer to generate *secA*(L187V)	CGCCATGTTGTCGCGCACGTA GTCAAAGCCGTA
X640	Forward mutagenic primer to generate *secA*(L187I)	TACGGCTTTGACTACATCCGCGACA ACATGGCG
X641	Reverse mutagenic primer to generate *secA*(L187I)	CGCCATGTTGTCGCGGATGTAG TCAAAGCCGTA
X642	Forward mutagenic primer to generate *secA*(M191F)	TACCTGCGCGACAACTTCGCGT TCAGCCCTGAA
X643	Reverse mutagenic primer to generate *secA*(M191F)	TTCAGGGCTGAACGCGAAGTTGT CGCGCAGGTA
X806	Forward phoA primer annealing at Thr 23, inserting at NdeI and HindIII restriction sites	GGGAATTCCATATGAAGCTTACA CCAGAAATGCCTGTTCTGGAA
X901	Forward mutagenic primer to generate *secA*(L187A)	TACGGCTTTGACTAC**GCG**CGCG ACAACATG
X911	Reverse mutagenic primer to generate *secA*(A373V)	GTGATCGA**AAC**CAGCGTTTGGTTTTC
X930	Forward mutagenic primer to generate *secA*(H484A)	TGAACAACGCCAAATTC**GCC**GCCAACG AAGCG
X936	Reverse phoA primer annealing at Thr 122, inserting a XhoI site, a Tyrosine and a stop codon	GACCCGCTCGAG**TTAATA**GGTGACG TAGTCCGGTTTG
X1021	Reverse mutagenic primer to generate *secA*(T340A/G341A/R342A)	CCCTGCATGGT**AGCAGCGGC**GTG TTCGTC
X1768	Forward mutagenic primer to generate *secA*(L464C)	CCATCGAAAAATCGGAGTGCGTGTCAA ACGAACTG
X1769	Reverse mutagenic primer to generate *secA*(L464C)	CAGTTCGTTTGACACGCACTCCGAT TTTTCGATGG
X2373	Forward mutagenic primer to generate *secA*(E487A)	AAATTCCACGCCAACGCCGCGGCGA TTGTTGCT
X2374	Reverse mutagenic primer to generate *secA*(E487A)	AGCAACAATCGCCGCCGGGTTGG CGTGGAATTT

Recombinant DNA

Gene	Uniprot accession number	Plasmid name	Vector	Description/source/reference
secA	P10408	pIMBB1280	pET3a	(Gouridis et al., 2013)
His *secA 6-901*	P10408	pIMBB7	pET5a	(Gouridis et al., 2013)
-		pLMB0081	pET3a	pIMBB1280 was digested with NcoI, the *secA* N31-898 fragment was removed, the plasmid was re-ligated and used for *secA* NcoI fragment cloning
secA(Δα0/α1-6A)	P10408	pIMBB1286	pET3a	also called mSecA (Gouridis et al., 2013)
secA(V280C/L464)	P10408	pLMB1646	pET3a	also called SecA-D2 (Vandenberk et al., 2019)
His *secA* cys-	P10408	pLMB1791	pET16b	(Krishnamurthy et al., 2021)
His *secA* cys- (V280C/L464)	P10408	pLMB1819	pET16b	(Krishnamurthy et al., 2021)
His *secYEG*	P0AGA2	pIMBB336	pET610	Gift from A. Driessen, University of Groningen, Groningen (van der Does et al., 1998)
	P0AG96			
	P0AG99			
His $secY_{PrlA4}EG$	P0AGA2	pIMBB842	pET610	(Gouridis et al., 2013)
	P0AG96			
	P0AG99			

secA$_{PrlD23}$	P10408	pIMBB1314	pET3a	also called PrlD23 Prl derivative of SecA with the Y134S mutation (Huie and Silhavy, 1995) introduced in secA 1–901 (Gouridis et al., 2013)
secA(H484Q)	P10408	pLMB1858	pET5a	Type I Prl derivative of SecA. *secA* N31-898 (H484Q) fragment from pIMBB578 (His SecA(H484Q) was inserted in pLMB0081 after NcoI digestion
His *secA*cys- (V280C/L464C/H484Q)	P10408	pLMB1907	pET16b	The mutation H484Q was introduced in pLMB1819 using primer pairs X2154-X2155
secA(H484A)	P10408	pLMB1859	pET5a	Type I Prl derivative of SecA. *secA* N31-898 (H484A) fragment from pIMBB527 (His SecA -H484A) was inserted in pLMB0081 after NcoI digestion
His *secA*cys- (V280C/L464C/H484A)	P10408	pLMB2027	pET16b	The mutation H484A was introduced in pLMB1819 using primer pairs X930-X2238
secA(L187A)	P10408	pLMB1860	pET5a	(Krishnamurthy et al., 2021)
His *secA*cys- (V280C/L464C/L187A)	P10408	pLMB1910	pET16b	(Krishnamurthy et al., 2021)
His *secA*cys- (V280C/L464C/A373V)	P10408	pLMB2107	pET16b	The mutation A373V was introduced in pLMB1819 using primer pairs X409-X911
His *secA* N6-901 (L187A)	P10408	pIMBB680	pET5a	The mutation L187A was introduced in pIMBB7 using primer pairs X403-X901
His *secA* N6-901 (L187V)	P10408	pIMBB946	pET5a	The mutation L187V was introduced in pIMBB7 using primer pairs X638-X639
His *secA* N6-901 (L187I)	P10408	pIMBB947	pET5a	The mutation L187I was introduced in pIMBB7 using primer pairs X640-X641
His *secA* N6-901 (A373V)	P10408	pIMBB687	pET5a	The mutation A373V was introduced in pIMBB7 using primer pairs X409-X911
His *secA* N6-901 (A373I)	P10408	pIMBB945	pET5a	The mutation A373I was introduced in pIMBB7 using primer pairs X636-X637
His *secA* N6-901 (A373F)	P10408	pIMBB944	pET5a	The mutation A373F was introduced in pIMBB7 using primer pairs X634-X635
secA "LO" or His *secA* N6-834 (C98A/P301C/S830C)	P10408	pIMBB941	pET5a	(Chatzi et al., 2017; Sardis et al., 2017)
secA "LC" or His *secA* N6-834 (K268C/I597C)	P10408	pIMBB1394	pET5a	(Chatzi et al., 2017; Sardis et al., 2017)
His *secA* N6-901 (TGR$_{342}$AAA)	P10408	pIMBB701	pET5a	The mutations T340A/G341A/R342A were introduced pIMBB07 using primer pairs X423-X1021 and X1768-X1769
secA(E487A)	P10408	pLMB2110	pET3a	The mutation E487A was introduced in pIMBB1280 using primer pairs X2373-X2374
proPhoA$_{1-122}$ -His	P00634	pIMBB1153	pET22b	*prophoA* N1-122 fragment was isolated from pIMBB977 (*prophoA* Δcys His) using primers X560-X936 and inserted in pet22b after NdeI-XhoI digestion.
PhoA$_{23-122}$-his	P00634	pIMBB1183	pET22b	*phoA* N23-122 fragment was isolated from pIMBB882 (*prophoA* His) using primers X806-X936 and inserted in pet22b after NdeI-XhoI digestion.
His *secA* N6-901 (E181A)	P10408	pIMBB677	pET5a	The mutation E181A was introduced in pIMBB7 using primer pairs X395-X400-X182
His *secA* N6-901 (F184A)	P10408	pIMBB678	pET5a	The mutation F184A was introduced in pIMBB7 using primer pairs X395-X401-X182
His *secA* N6-901 (D185A)	P10408	pIMBB679	pET5a	The mutation D185A was introduced in pIMBB7 using primer pairs X395-X402-X182

His *secA* N6-901 (R188A)	P10408	Pimbb681	pET5a	The mutation R188A was introduced in pIMBB7 using primer pairs X395-X404-X182
His *secA* N6-901 (D189A)	P10408	pIMBB682	pET5a	The mutation D189A was introduced in pIMBB7 using primer pairs X395-X405-X182
His *secA* N6-901 (M191A)	P10408	pIMBB683	pET5a	The mutation M191A was introduced in pIMBB7 using primer pairs X395-X406-X182
His *secA* N6-901 (M191F)	P10408	pIMBB948	pET5a	The mutation M191F was introduced in pIMBB7 using primer pairs X642-X643

Software and algorithms		
Masslynx V4.1	Waters	www.waters.com
DynamX 3.0	Waters	www.waters.com
PyHDX 0.3.0	(Smit et al., 2021a, 2021b, 2021c)	https://github.com/Jhsmit/PyHDX
Frustratometer Server	(Parra et al., 2016)	http://frustratometer.qb.fcen.uba.ar/
WEBnm@ server	(Tiwari et al., 2014)	http://apps.cbu.uib.no/webnma3
MobiDB	(Piovesan et al., 2021)	https://mobidb.bio.unipd.it/
Origin	OriginLab	https://www.originlab.com/index.aspx?go=Products/Origin
Matlab (R2014b/R2017b)	MathWorks	www.mathworks.com/products/matlab
Pymol	Schrödinger	https://pymol.org/2/
Prism 5.0	Graphpad	www.graphpad.com/scientific-software/prism/

Other		
Ni+2-NTA Agarose resin	Qiagen	Cat# 30250
ACQUITY UPLC BEH C18 Column, 130 Å, 1.7 μm, 1 mm × 100 mm	Waters	Cat# 176000862
ACQUITY UPLC BEH C18 VanGuard Pre-column, 130 Å, 1.7 μm, 2.1 mm × 5 mm	Waters	Cat# 186003975
Superdex 200 10/300 GL	GE healthcare	Cat# 28990944
Superdex 200 26/600	GE healthcare	Cat# GE28-9893-36
Sepharose CL-6B	GE healthcare/Cytiva	Cat# 17016001

RESOURCE AVAILABILITY

Lead contact

Further information and requests for reagents may be directed to, and will be fulfilled by the lead author, Dr. Anastassios Economou (tassos.economou@kuleuven.be).

Materials availability

This study did not generate new unique reagents.

Data and code availability

- HDXMS raw mass spectra files, MD simulations and smFRET raw data files described in this study have not been deposited in a public repository because of the large data sizes but are available from the lead contact on request.
- This paper does not report original code.
- Any additional information required to reanalyze the data reported in this paper is available from the lead contact upon request

EXPERIMENTAL MODEL AND SUBJECT DETAILS

E. coli T7 express lysY/I^q [derivative of BL21 (DE3)] cells transformed with the relevant protein gene (key resources table) were grown at 37°C in 5 L flasks until OD_{600} 0.6–0.7 was reached. Protein expression was induced with 0.2 mM IPTG and cells were grown at 30°C

for a further 3 h. Cells were collected by centrifugation (5,000 × g; 4°C; 15 min; Avanti J JLA8.1000 rotor) and lysed in a French Press (8,000 psi; 3–5 passes; 4°C).

METHOD DETAILS

For buffers, strains, plasmids and primers see STAR Methods and key resources table.

List of buffers

Buffer	Composition
A	50 mM Tris-HCl, pH 8.0, 50 mM NaCl, 6 m Urea, 50% v/v glycerol
B	50 mM Tris-HCl pH 8.0, 50 mM KCl, 1 mM $MgCl_2$, 1 mM DTT
C	50 mM Tris-HCl pH 8.0, 50 mM KCl, 1 mM $MgCl_2$, 4 μM $ZnSO_4$, 2 mM TCEP
D	1.3% formic acid, 4 mM TCEP, 1 mg/mL fungal protease XII
E	50 mM MOPS pH 7.0, 50 mM KCl, 1 mM $MgCl_2$, 4 μM $ZnSO_4$, 2 mM TCEP

Molecular cloning

Site directed mutagenesis was performed using QuickChange site directed Mutagenesis protocol (Stratagene Agilent) using indicated vector templates and primers. Molecular cloning and sample handling was as previously described (Krishnamurthy et al., 2021)

Protein purification

SecA and derivatives were overexpressed in T7 Express lysY/I^q [derivative of BL21 (DE3)] cells and purified as described (Papanikolau et al., 2007). Briefly, SecA and its derivatives were affinity purified at 4°C on a home-made Cibacron-Blue resin column (Sepharose CL-6B, GE healthcare) and subsequently cleaned up in two consecutive gel filtration steps (HiLoad 26/600 Superdex 200 pg; GE healthcare). All proteins were assessed for purity on SDS-PAGE. The His-tagged derivatives of $SecA_{V280C/L464C}$ (variant of SecA used for smFRET experiments), $proPhoA_{1-122}$ and $PhoA_{23-122}$ were purified on Ni^{+2}-NTA agarose columns as previously described (Chatzi et al., 2017; Vandenberk et al., 2019). His-$SecA_{V280C/L464C}$ were stored as described (Krishnamurthy et al., 2021), while $proPhoA_{1-122}$ and $PhoA_{23-122}$ were stored in buffer A (Chatzi et al., 2017).

SecYEG-IMVs (inverted membrane vesicles) and derivatives were prepared as in (Lill et al., 1989, 1990) and concentration was determined as described (Gouridis et al., 2013). All biochemicals were tested for functional activity in ATPase and *in vitro* preprotein translocation assays.

MANT-ADP release assays

MANT-ADP release assays were carried out as described in (Krishnamurthy et al., 2021). SecYEG:$SecA_2$ (0.5 μM) were added to free MANT-ADP (1 μM; 30 s) to initiate MANT-ADP binding onto the translocase. Client proteins were added (chase; 90 s) at the following final concentrations: $proPhoA_{1-122}$ – 15 μM; $PhoA_{23-122}$ – 20 μM; signal peptide – 30 μM. Fluorescence intensity traces were recorded for 5 min on a Cary Eclipse Fluorimeter (Agilent) with λ_{ex} = 356 nm and λ_{em} = 450 nm (excitation slit = 2.5 nm; emission slit = 5 nm). Experiments were carried out in Buffer B.

Dynamics of the Sec translocase by HDX-MS

HDX-MS experiments were carried out as previously described (Krishnamurthy et al., 2021). SecA and derivatives were diluted into buffer B to a final concentration of ~100 μM prior to HDX-MS analysis. To monitor SecA:$proPhoA_{1-122}$ interactions in solution, $proPhoA_{1-122}$ (in Buffer A) was diluted in buffer B to a final concentration of 250 μM (0.2 M Urea), immediately added to SecA at 4 μM: 35 μM ratio (SecA: $proPhoA_{1-122}$) and incubated for 2 min prior to D exchange. Complexes of the channel with SecA and its derivatives were generated and analyzed as described (Krishnamurthy et al., 2021). Briefly, sonicated SecYEG IMVs were incubated with SecA at a molar ratio of 1.5:1 (SecY:SecA) for 2 min on ice. To monitor how signal peptides (SP) activate the translocase, the synthetic proPhoA SP (Genescript; 45 mM in 100% DMSO) was diluted 30-fold into Buffer B (to obtain 1.5 mM SP in 3% DMSO), added to preincubated SecA:SecYEG at a final molar ratio of 4 μM: 6 μM: 30 μM (SecA:SecYEG:SP) and the reaction was incubated for a further 1 min.

SecYEG:SecA:client interactions: To monitor the dynamics of SecA as part of SecYEG:SecA:client complexes, the client ($proPhoA_{1-122}$ and $PhoA_{23-122}$) were added in excess to preincubated SecYEG:SecA to maintain a final molar ratio of 4 μM: 6 μM: 20 μM (SecA:SecYEG:client). In SecYEG:SecA: signal peptide + mature domain complexes, proPhoA signal peptide was added to preincubated SecYEG:SecA:$PhoA_{23-122}$ (as described above) to a final concentration of 30 μM. Indicated concentrations are in the final D-exchange reaction. The D-exchange initiated by 10-fold dilution of the reaction in D_2O buffer C (90% final D_2O concentration; pH_{read} 8.0) with fresh TCEP added at 2 mM, at 30°C, for 7 timepoints (10 s, 30 s, 1 min, 2 min, 5 min, 10 min, 30 min), in 3–4 technical replicates (Table S1). Reactions were quenched in pre-chilled buffer D at a 1:1 ratio (final pH of 2.5) and proteolyzed by soluble fungal protease XIII (1 mg/mL). The quenched samples were centrifuged at 20,000 × g, for 90 s, at 4°C, on a benchtop centrifuge (Eppendorf). Pellet was removed and the supernatant, containing peripheral membrane protein peptides (i.e. SecA and clients), were subsequently subjected to a second protease step on a home-packed pepsin column attached to a nanoACQUITY UPLC system with HDX technology (Waters, UK). Peptides were analyzed on a Synapt G2 ESI-Q-TOF mass spectrometer. HDX-MS data were acquired and analyzed as previously described (Krishnamurthy et al., 2021). All mutant proteins were handled similarly to the wild type ones and reactions were maintained at similar molar ratios.

HDX-MS data visualization

HDX-MS data are mapped and visualized onto the closed-clamp structure of SecA derived from MD simulations (unless otherwise stated) with the helicase motor and its gate2 (motifs Ia, IVa) in the open state (Krishnamurthy et al., 2021). Only one protomer of the dimer is shown, for simplicity. D-uptake differences between reference state (top pictogram) and test state (bottom pictogram) are mapped in colors of purple and green. Decreased dynamics effects are shown in shades of purple and increased dynamics effects are shown in shades of green. Regions showing no difference are in transparent gray. For certain comparisons, these data are also presented as linear bars (see Figure S6).

Dynamics of client proteins by HDX-MS

To monitor dynamics of free $proPhoA_{1-122}$ and $PhoA_{23-122}$, proteins were diluted from 6 M urea into buffer B to a final concentration of 50 μM, and subsequently diluted 10-fold into D_2O buffer E. D-labeling was carried out for a short 10 s pulse at 4°C.

To monitor dynamics of client proteins when bound to the Sec translocase (see Figure S7A for experimental schematic) we had to ensure all available client proteins were bound to translocase thus, the concentration of client proteins was maintained sub stoichiometric to the translocase. Prior to D-exchange, the complete SecYEG:SecA; preprotein complex was generated by pre-incubating $SecA_2$ (20 μM) with SecYEG (40 μM) for 5 min on ice. Client proteins were added to a final concentration of 15 μM and incubated further for 5 min on ice. The complex was incubated for 20 s at 37°C (this step was omitted for low temperature experiments). The D-exchange initiated by diluting the complex 10-fold in D_2O buffer C. Labeling was carried out for 10 s at 4°C. Reaction was quenched using buffer D, proteins were proteolyzed and injected into an HDX sample manager (Waters, Milford) for UPLC based peptide separation as described (Krishnamurthy et al., 2021). To unambiguously detect the low abundance peptides from the client proteins, data acquisition was carried out in $UDMS^E$ data acquisition mode with Ion mobility separation feature turned on. Data acquisition parameters (Cryar et al., 2017) and peptide analysis/quantification (Krishnamurthy et al., 2021) were as described.

Determination of ΔG_{ex} values

ΔG_{ex} values were determined using PyHDX software (v0.4.0-rc1) (Smit et al., 2021a). D-uptake data from triplicate experiments, for all timepoints were input along with 100% deuteration control. Input parameters were set to the following parameters: temperature - 303 K; ph – 8; stop loss – 0.01; stop patience – 100; learning rate – 10; momentum – 0.5; epochs – 100,000; regularizer 1–0.01, regularizer 2–0.01.

Single-molecule fluorescence microscopy and PIE

Protein purification, fluorescent labeling, sample preparation and data analysis, quantification and statistical analysis for single molecule PIE based FRET experiments were carried out as previously described (Krishnamurthy et al., 2021). In brief, His-$SecA_{V280C/L464C}$ (Table S5) was labeled with Alexa 555-maleimide and Alexa 647-maleimide (Thermo Fisher Scientific) and purified by analytical gel filtration (Superdex 200 Increase PC 10/300; GE healthcare). A labeling efficiency of >80% was estimated based on protein absorbance and fluorescence intensities. Single-molecule PIE experiments were performed using the MicroTime 200 (Picoquant, Germany). Confocal scanning analysis mode was applied to follow the conformational dynamics of SecA in solution at 20°C. To follow the smFRET dynamics of dimeric SecA, His-SecA (50–100 pM) was stochastically labeled at $V280C_{PBD}/L464C_{NBD2}$ with Alexa 555/Alexa 647 (blue circle) and was subsequently dimerized with excess cold SecA (1 μM) to $SecA_2$ with a single fluorescent protomer. To follow the effect of signal peptide binding on clamp dynamics of the translocase, signal peptide was added to monomeric, dimeric or channel-primed SecA [generated as described (Krishnamurthy et al., 2021)] to a final concentration of 37 μM. $proPhoA_{1-122}$ was added to a final concentration of 10 μM. All mutant derivatives were handled similarly to wild-type proteins.

H-bonding graph analysis

To determine H-bond paths and long-distance conformational couplings between the signal peptide binding cleft and gate2, we used algorithms based on graph theory and centrality measures as described (Karathanou and Bondar, 2019; Krishnamurthy et al., 2021).

Briefly, residues were considered H-bonded if the distance between the hydrogen and acceptor heavy atom, d_{HA}, is $\leq$2.5 Å. H bonds were calculated between protein sidechains, and between backbone groups and protein sidechains. Data are visualized as H-bond networks with unique lines (colored according to H-bond frequency) between Cα atoms of residue pairs that H-bond. H-bond frequency is the percentage of analyzed trajectory segment during which two residues are H-bonded.

Normal mode analysis and intrinsic disorder prediction

Normal modes that describe protein vibrational movements, were calculated using the WebNM@ web server (Tiwari et al., 2014) with PDB: 2VDA as the input structural model of SecA. Per-residue displacement and normal mode flexibility were derived from normal mode eigenvalues as described (Dobbins et al., 2008; Smit et al., 2021b). Total vibrational displacement of each residue undergoing fluctuations under low frequency normal modes (modes 7–12) are calculated and plotted. Residues that undergo displacement greater than 2 are highlighted in shades of blue.

Intrinsic disorder prediction was carried out in the MobiDB online tool using the SecA uniprot code as input sequence (https://mobidb.bio.unipd.it/P10408). Numerous other intrinsic disorder prediction tools (PONDR, DisEMBL, flDPnn, SPOT-Disorder2 and IUPred3) were also tested using the SecA sequence as the input sequence (Erdos et al., 2021; Hanson et al., 2017; Hu et al., 2021; Linding et al., 2003; Peng et al., 2005; Piovesan et al., 2021).

Miscellaneous

Pymol (https://pymol.org/) was used for structural analysis and visualization. SecA activation energy determination, *in vivo* proPhoA and PhoA translocation, *in vitro* proPhoA translocation, SecA ATPase activity, *in vivo* SecA complementation, affinity determination of SecA and/or proPhoA for the translocase, were as described (Chatzi et al., 2011; Gouridis et al., 2009, 2010, 2013). H-bond networks between the signal peptide cleft and motif IVa were determined as described (Krishnamurthy et al., 2021). ADP:BeF_X was generated by adding ADP:$BeCl_2$:NaF in a 1:1:5 ratio and incubated at 4°C for 30 min to obtain a final concentration of 50 mM.

QUANTIFICATION AND STATISTICAL ANALYSIS

MANT-ADP release assays

For MANT-ADP assays, 3–4 replicate measurements were carried out for each condition. Raw fluorescence data from all replicates are summed and presented as transparent traces that indicate the spread of the distribution. Also, data were averaged and smoothened using cubic spline smoothening and presented as solid traces (GraphPad Prism 5). Data are independently normalized using the fluorescence intensity of free MANT-ADP (at 30 s) as 0% and translocase-bound MANT-ADP (at 45 s) as 100%.

HDX-MS data

D exchange experiments were carried out in at least 3 replicates (details in Table S1) and performed over multiple days in non-sequential order to account for instrumental variations. All spectra were individually inspected and manually curated. A difference of ±0.5 Da between different states was considered significant (Houde et al., 2011). Comparison between different states of SecA was carried out by considering one state as the control and the other as the test state. Deuterium uptake data were converted to %D-uptake values before comparison between states. In pairwise comparison of states, differences were considered significant if they satisfied two criteria: a) $\geq$ 0.5 Da absolute difference in deuterium exchange, b) $\geq$ 10% D-uptake difference. Differences between states were further classified into minor (10%–20% difference in % D-uptake) or major ($\geq$20% difference in % D-uptake) differences.

Biochemical assays

All biochemical *in vitro* and *in vivo* assays were carried out in 3–6 biological replicates. Data was quantified and presented as bar graphs with error bars signifying the SEM.

For *in vivo* proPhoA translocation assays, secreted phosphatase units were converted to protein mass (Gouridis et al., 2010). Mean values from 6 replicates are presented as bar graphs with error bars signifying SEM.

For *in vitro* ATPase assays freely diffusing SecA or SecA derivative (basal; B), in SecYEG-bound conditions (membrane; M) 1 μM of SecYEG in IMVs are added and in translocating (T) conditions 9 μM proPhoACys$^-$ is added to the complex as described (Gouridis et al., 2010). Data are the average of 3–6 replicate measurements and presented as bar graphs with error bars signifying SEM.

smFRET data

FRET histograms from 3–5 replicate experiments (independent protein purification and sample labeling) were fitted with a Gaussian mixture model with restricted standard deviation. Histograms were fitted with 3 Gaussian distributions corresponding to 'Wide-open' (apparent FRET 0.47), 'Open' (apparent FRET 0.65) and 'Closed' (apparent FRET 0.78) clamp states. The amplitude of each population distribution corresponds to the abundance of the respective conformational states. These data are presented as bar graphs with SEM. The mean and amplitude of each distribution was calculated with Origin software version 2018 (OriginLab).